# Variable magnetic field technology and permanent magnet characteristic by the request of electric traction motors

H. Nakai*

(Toyota Central R&D Labs., Inc.)

A traction electric motor of HV, PHV and EV is required high efficiency to reduce fuel consumption. While, to secure passengers space, the motor is also demanded downsizing. Since the motor is in the industrial products, low-cost is also required without doubt. The motor requests a several characteristic of a permanent magnet for fulfilling above 3 demands. In order to downsize the motor, firstly, we need a high magnetic flux density magnet (a strong magnet) and a magnet which is hard to demagnetize. The motor is often put in a small space for which it is easy to be filled with heat, for example, an engine compartment. The motor which uses a strong magnet can produce large torque, even though the motor is put in a small space. The motor is often cooled using by a transmission fluid to prevent temperature rise. Even if the motor is chilled using the fluid, the temperature is more than 100℃. Therefore, the magnet which is hard to demagnetize in high temperature is desired in the motor. Almost traction motors use a Nd-Fe-B sintered permanent magnet in order to fulfil the demand of minimization and demagnetization. It is, however, a problem that the Nd-Fe-B magnet has high cost price. Reducing the cost of the Nd-Fe-B magnet is a 2nd request of the motor. In order to realize high efficiency which is a 3rd demand for the motor, we request high electrical resistance magnet and variable magnetic field magnet. Cyclical change of magnetic resistance caused by stator tooth make a magnetic flux change in a magnet placed in the motor. An eddy current occurred by the magnetic flux change makes loss in a magnet. High electrical resistance of a magnet avoids eddy current and reduces the loss. Reduction of the loss achieves increasing motor efficiency. Maximum torque of the motor determines a magnet force in many situations. However, the magnet force is often too strong to achieve high efficiency in high rotational speed and small load area. The efficiency in this area has great influence on fuel consumption of a vehicle. Therefore, variable magnetic field magnet is desired to improve efficiency. The strength of a Nd-Fe-B magnet is also fixed like other permanent magnets. The motor used in vehicle replaces a part of magnet torque with reluctance torque to carry out variable magnetic field. Reluctance torque is not, however, large enough to replace all magnet torque. So, last 10 years several studies which achieve variable magnetic field using not only reluctance torque but also new mechanisms have been done actively. As one kind of studies which achieve variable magnetic field, there is a motor which controls permanent magnetic force[1]. The advantage of this motor is that the structure is almost same with an ordinary IPM motor. The disadvantage is vibration occurred by pulse current which is used for controlling magnet force. Changing magnetic resistance method using mechanical way[2] is one of a variable magnetic field study. The advantage of this method is that the magnetic field can be accurately measured using a mechanical air-gap. The motor needs, however, a mechanical actuator. This actuator is a weak point. Other method controlling magnetic force has an electromagnet in addition to a permanent magnet. This method has ability changing magnetic force quickly because of an electromagnet. An electromagnet needs space bigger than a permanent magnet. Therefore, it is a problem to increase the size of the motor. There is a study solving this problem in order to achieve downsizing with high efficiency[3]. The proposed motor in Fig. 1 constitutes a 3-DOF magnetic circuit with dust core. The circuit has one radial air-gap and two axial air-gaps to increase torque density. This motor settles an excited field coil of an electromagnet in the gap of a radial and an axial air-gap not to increase the size. Therefore, this motor can achieve variable magnetic field with downsizing. As mentioned as above, traction motor demands various performances to a magnet. A magnet that satisfies all performance has not yet been developed. Development of a higher-performance magnet will improve characteristic of the motor and realize restraint of the global warming.

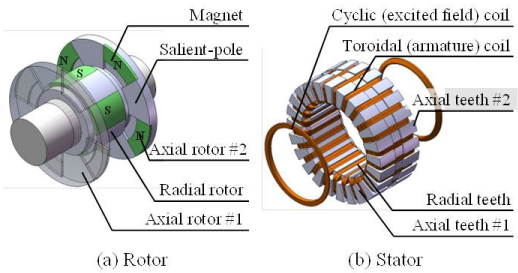


**Fig. 1**　3 air-gaps motor with excited field coils.

## References

1) K. Sakai et al., *IEEJ Transactions on Industry applications*, **Vol.131**, **No.1**, pp.53-60 (2011) (in Japanese).
2) H. Nakai et al., *JIASC2007*, **No.3-64**, pp.337-342 (2007) (in Japanese).
3) M. Namba et al., *IEEJ Transactions on Industry applications*, **Vol.135**, **No.11**, pp.1085-1090 (2015) (in Japanese).

# Development of Measurement Technique of Three-dimensional Demagnetization Distribution in Permanent Magnets for Motors

Y. Asano, S. Araki, A. Yamagiwa
(Technology Research Association of Magnetic Materials for High-Efficiency Motors (MagHEM))

It is important to estimate the demagnetization state in the magnets in Interior Permanent Magnet Synchronous Motors (IPMSMs), which are often used for consumer electronics and HEV traction motors . However, the distribution of demagnetization in permanent magnets for these motors is not uniform due to the difference of coercivity of local parts in the magnet material and the difference of the working point of local parts in the magnet caused by the variation of magnetic circuit in a motor. So, it was necessary to estimate the demagnetization distribution in the magnet by FEA, because there were not techniques to measure that. Therefore, we develop a method to evaluate the three-dimensional demagnetization state including the inside the magnet by cutting the magnet into the cubes, as shown in Fig. 1, and measuring the B–H characteristics of each magnet cube using Vibrating Sample Magnetometers (VSM), as shown in Fig. 2. At first we lock the motor rotation in high temperature environment, and an electric current is applied into a coil to hang opposing magnetic field. Next, magnets are taken out from the motor. Then, we cut the magnet into the cubes without demagnetizing anymore. Finally, we measure the B–H characteristics of each magnet cube shown as in Fig. 3 and , formula[1] and calculate demagnetizing ratio distribution.

$$\text{Demagnetizing ratio}[\%]=(B1-B2)/B1\times 100 \quad [1]$$

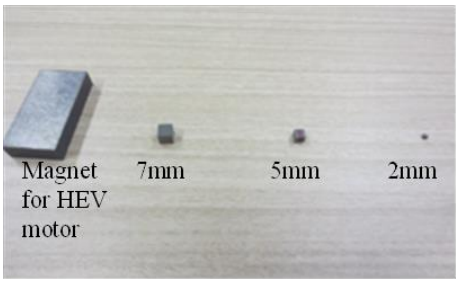


Fig.1. Magnet cut into cubes

Fig. 2. Vibrating Sample Magnetometers VSM

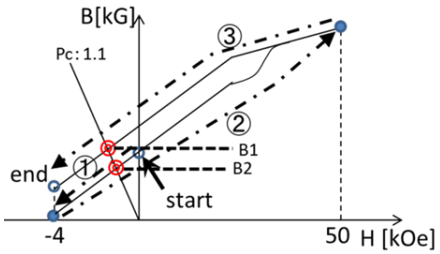


Fig.3. Calculation method of demagnetizing ratio

Reference

1) S. Araki, Y. Asano, A. Yamagiwa, “Development of Measurement Technique of Three-dimensional Demagnetization Distribution in Permanent Magnets for Motors (Part 1)” The paper of joint Technical Meeting on Rotating Machinery, Linear Drive and Home and Consumer Appliances, IEE Japan, RM-15-083/LD-15-034/HCA-15-036(2015)

# Grain size refinement of Nd-Fe-B sintered magnets

Y. Une, H. Kubo, T. Mizoguchi, T. Iriyama and M. Sagawa

(Intermetallics Co., Ltd. (Technology Research Association of Magnetic Materials for High-Efficiency Motors / Nagoya Branch), Creation-Core Nagoya 101, 2266-22 Anagahora, Shimo-shidami, Moriyama-ku, Nagoya, Aichi 463-0003, Japan)

High remanence and large coercivity are required for Nd-Fe-B magnets in high-efficiency motors such as traction motors for EV or HEV. The addition of Dy is the most common way to increase the coercivity of Nd-Fe-B magnets. The problem of the Dy addition is the reduction of the remanence or the rise of material cost. Accordingly, efforts to reduce Dy use have been undertaken all over the world. One of the important idea to reduce the Dy use is a grain size refinement of $Nd_2Fe_{14}B$ crystal. Also, optimizing the grain boundary structure is necessary to achieve the large coercivity. We have been challenging the grain size refinement of Nd-Fe-B sintered magnets since 2007.

From 2007 to 2012, we had developed under “Rare Metal Substitute Materials Development Project” commissioned by the New Energy and Industrial Technology Development Organization (NEDO). In this project, we obtained fine powder with average particle size of around 1 μm using a helium jet-milling[1]. We fabricated the fine grained Dy-free Nd-Fe-B magnets using this powder with coercivity of around 20 kOe; about 40% of Dy can be saved by this technique.

Then, from 2012 to now, we have been challenging to develop the new production process for the further grain size refined Dy-free Nd-Fe-B sintered magnets under "Future Pioneering Projects / Development of magnetic material technology for high-efficiency motors" commissioned by NEDO.

The sub-micron grained sintered magnet was developed using both HDDR process and helium gas jet-milling[2]. This magnet (HDDR sintered magnet) had a better temperature coefficient of coercivity than the conventional sintered magnet. However, the coercivity at room temperature is around 13 kOe which is rather lower than we expected[3]. It can be seen that the HDDR sintered magnet has thinner Nd-rich grain boundary phase with around 1 nm than that of conventional magnet (thickness: 2 nm). We have been trying to expand the grain boundary phase of the HDDR sintered magnets by various methods such as the grain boundary diffusion (GBD) technique. One of the results is shown in Fig.1.

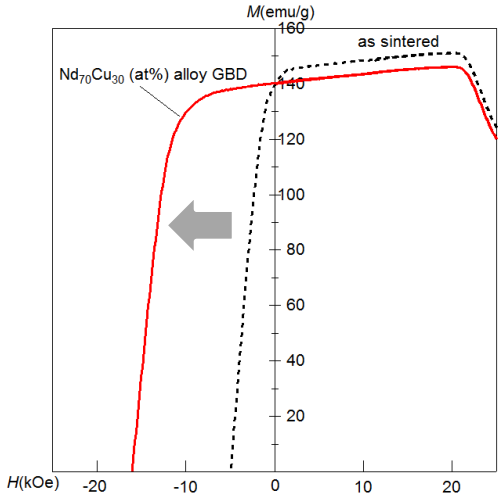


Fig.1 GBD for the HDDR sintered magnets

References

1) Y. Une and M. Sagawa, J. Jpn. Inst. Met. **76**, 12 (2012) (in Japanese)
2) M. Nakamura, M. Matsuura, N. Tezuka, S. Sugimoto, Y. Une, H. Kubo, and M. Sagawa, Appl. Phys. Lett. 103 (2013) 022404.
3) Y. Une, H. Kubo, T. Mizoguchi, T. Iriyama, M. Sagawa, M. Nakamura, M. Matsuura, and S. Sugimoto, The 38th Annual Conference on MAGNETICS in Japan (2014), 2pB-2

# Newly developed $(R,Zr)(Fe,Co)_{12-x}Ti_x$-$N_y$ compounds for permanent magnets (y=1.3 for R=Nd, y=0 for R=Sm)

K. Kobayashi, S. Suzuki, T. Kuno and K. Urushibata
(Shizuoka Institute of Science and Technology, Toyosawa 2200-2, Fukuroi, Shizuoka 437-8555, Japan)

$(R_{0.7\text{-}0.8}Zr_{0.3\text{-}0.2})(Fe_{0.75}Co_{0.25})_{11.5}Ti_{0.5}$ (R = Nd and Sm) alloys for permanent magnet materials were prepared by strip-casting. The homogeneity of the elements detected using electron-probe micro-analysis (EPMA) was fairly good. The occupation sites of the substituted elements, i.e. Zr in R sites, Ti in Fe(8i) sites and Co in Fe(8j) and Fe(8f) sites, were revealed by using spherical aberration-corrected scanning transmission electron microscopy (Cs-STEM). The stabilization of $ThMn_{12}$ structure at a low Ti content of $Ti_{0.5}$ mainly originated from the substitution of R sites with Zr. The nitrogenated R = Nd alloy, $(Nd_{0.7}Zr_{0.3})(Fe_{0.75}Co_{0.25})_{11.5}Ti_{0.5}N_{1.30}$ compound, showed good magnetic properties of $J_s$ = 1.67 T and $H_a$ = 5.25 MA/m at room temperature (RT). The R = Sm alloy, $(Sm_{0.8}Zr_{0.2})(Fe_{0.75}Co_{0.25})_{11.5}Ti_{0.5}$, also had $J_s$ = 1.58 T and $H_a$ = 5.90 MA/m at RT. The values in the R = Sm alloy were still $J_s$ = 1.50 T and $H_a$ = 3.70 MA/m at 473 K, and were higher than those of $Nd_2Fe_{14}B$ phase at the temperature [1]-[6]. Because the R = Sm alloy is a Dy-free and N-free powder, it is a promising candidate as a material for sintered magnets (4).

For the measurement of magnetic properties of the samples, physical properties measurement system-vibrating sample magnetometer (PPMS-VSM) under a maximum applied field of 9 T was employed. Especially, the $J_s$ and $H_a$, i.e. $K_1$, was calculated from the magnetization curve using the law of approach to saturation (LAS) method. The sample powder consisted of secondary grains composed of isotropic agglomerated primary grains of about 5×5~20 μm. The sample powder was mixed in epoxy resin, then the magnetically isotropic sample. The analysis was performed by using the following equation [7], [8].

$$dJ(H) / dH = J_S (8/15) (K_1^2/J_S^2) (1/H^3)) + \chi_0 \qquad (1)$$

Here, $J(H)$ is the measured polarization under applied field $H$, $J_S$ is the saturation polarization, and $K_1$ is the first-order anisotropy constant. Equation (1) was applied to the measured polarization under a high field of 6-9 T, and the plots between $dJ(H)/dH$ and $1/H^3$ are used to calculate $J_S$ and $K_1$ values. This method was used to obtain the results in our previous studies [1]-[4] . In the study [4] , however, we compared the results obtained using above equation (1) with those using $J(H)$ vs $1/H^2$ plots, and employed the latter method for the stability of obtained values. As mentioned above, the comparatively high magnetic properties in R=Nd nitrogenated compound and R=Sm alloy were measured using the LAS method.

Evaluating the α-(Fe,Co) phase concentrations in the samples is important for calculating precise $J_s$. We determined the volume fractions of the phase using two methods. First, we compared the largest XRD peak height of the α-(Fe,Co) phase around 2θ=44.5º with that of the main $ThMn_{12}$ phase of around 2θ=42.4º. The ratios of peak heights corresponded to the volume fractions of the phases. This method included the error from the crystallinity of each phase in the samples and the local distribution of the phases in the sample particles. Second, we obtained the volume fractions directly, through measuring the surface area fractions of the α-(Fe,Co) phase on the polished surface of electron back-scattering diffraction (EBSD) image of the sample particles. Each phase was clearly distinguished in this method, however, there were errors arising from the difference in the particles observed. Although numerous observations are required for this method, the number of observations was limited for some particles in the experiments.

The above $J_S$ values of samples were corrected using XRD data those for eliminating the contribution from α-(Fe,Co) phases. The obtained values were indicated in Fig.1. The values (a) were shown in our previous papers [1]-[4], and those of (b) were newly obtained in our recent measurements.

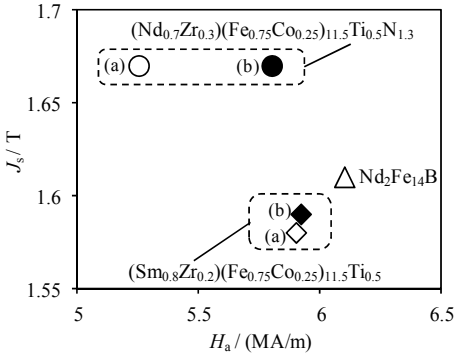


Fig. 1 Results of the LAS method using PPMS-VSM (at RT)

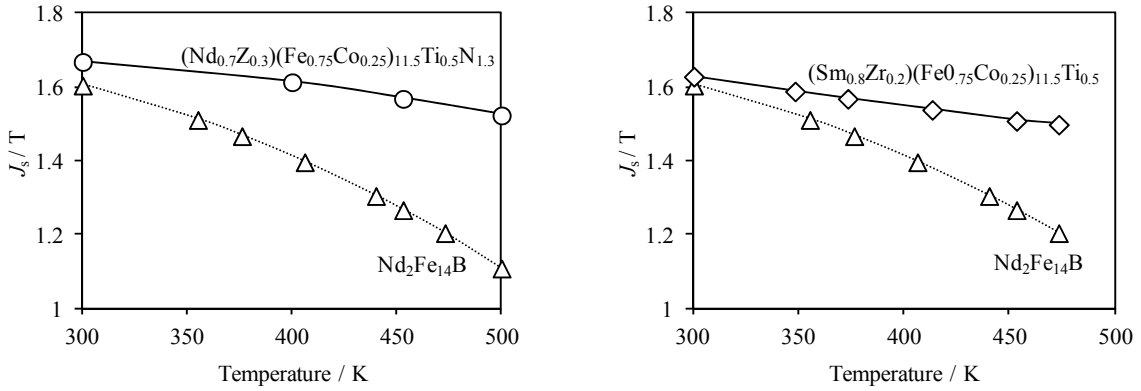


Fig. 2 Temperature dependences of $J_s$ in R=Nd compound (a) and in R=Sm alloy (b) with those in $Nd_2Fe_{14}B$ phase [6].

The Curie temperature ($T_c$) of the alloys was measured also using the PPMS-VSM with an maximum applied field of about 9 T. *T*c of $(Nd_{0.7}Zr_{0.3})(Fe_{0.75}Co_{0.25})_{11.5}Ti_{0.5}N_{1.30}$ compound is more than 840K that is sufficiently higher than that of an Nd-Fe-B magnet of about 584 K [5], [6]. The temperature dependences of $J_s$ (Fig. 2) and $H_a$ of the alloys showed that the $J_s$ and $H_a$ values at 473 K of $(Nd_{0.7}Zr_{0.3})(Fe_{0.75}Co_{0.25})_{11.5}Ti_{0.5}N_{1.30}$ compound and $(Sm_{0.8}Zr_{0.2})(Fe_{0.75}Co_{0.25})_{11.5}Ti_{0.5}$ alloy ($T_C$ estimated to be 880K) were higher than those of Nd-Fe-B (the figure for $H_a$ exists in ref.[4]). As mentioned above, $(Sm_{0.8}Zr_{0.2})(Fe_{0.75}Co_{0.25})_{11.5}Ti_{0.5}$ has still $J_s$ = 1.50 T and $H_a$ = 3.70 MA/m at 473K, and we would like to insist again that the alloy is Dy-free and N-free, therefore, it is a promising candidate for permanent magnet material for high-temperature applications.

**Acknowledgement**

This report is based on results obtained from the pioneering program “Development of magnetic material technology for high-efficiency motors” (2012–) commissioned by the New Energy and Industrial Technology Development Organization (NEDO).

**References**

[1] S. Suzuki, T. Kuno, K. Urushibata, K. Kobayashi, N. Sakuma, K. Washio, M. Yano, A. Kato, A. Manabe, J. Magn. Magn. Mater. vol.401 (2016) p.259-268.

[2] S. Suzuki, T. Kuno, K. Urushibata, K. Kobayashi, N. Sakuma, K. Washio, H. Kishimoto, A. Kato and A. Manabe, AIP Advances 4 (2014) 117131.

[3] N. Sakuma, S. Suzuki, T. Kuno, K. Urushibata, K. Kobayashi, M. Yano, A. Kato and A. Manabe, AIP Advances 6 (2016) 056023.

[4] T. Kuno, S. Suzuki, K. Urushibata, K. Kobayashi, N. Sakuma, M. Yano, A. Kato and A. Manabe, AIP Advances 6 (2016) 025221.

[5] M. Sagawa, S. Fujimura, N. Togawa, H. Yamamoto, and Y. Matsuura, J. Appl. Phys. 55 No.6 (1984) p.2083-2087.

[6] S. Hock, Ph.D. thesis, Ph.D thesis, Universität Stuttgart (1988).

[7] H. Kronmüller and M. Fähnle, Micromagnetism and the Microstructure of Ferromagnetic Solids, Cambridge (2003) p.174.

[8] G. Hadjipanayis, D.J. Sellmyer, and B. Brandt, Phys Rev., B 23 No.7 (1981) p.3349-3354.

# Research trends for the high-performance La-Co substituted M type ferrite magnets

Yoshinori Kobayashi
Hitachi Metals, Ltd.

## 1. Introduction

The hexagonal Sr-M type ferrite magnet has been widely used in applications such as the motor for car electrical equipments and for air conditioners and refrigerators. Recently, the magnetic properties of ferrite magnet has been improved by substituting La and Co for Sr and Fe atoms, respectively. The La-Co substituted M-type ferrites (Sr-La-Co M-type ferrite and Ca-La-Co M-type ferrite, to which we will refer as 'SLC-M' and 'CLC-M' hereafter)[1)-3)] are known to have the higher magnetic crystalline anisotropy compared with Sr-M type ferrite. In this study, the occupation sites of cobalt ions in the La-Co substituted M-type ferrite compound were analyzed by the neutron diffraction, the extended X-ray absorption fine structure (EXAFS) and the X-ray magnetic circular dichroism (XMCD) to understand the relationship between the local structure and the improvements of magnetic characteristics in the La-Co substituted M-type ferrite, and furthermore, microstructure of CLC-M sintered ferrite magnets were analyzed by Spherical Aberration Corrected Scanning Transmission Electron Microscopy (Cs-STEM) to get guiding principles for improving magnetic property.

## 2. Cation distribution analysis of La-Co M-type ferrites by neutron diffraction, EXAFS and XMCD[4), 5)]

We investigated the site distribution of the cobalt ions in SLC-M ($Sr_{0.7}La_{0.3}Co_{0.3}Fe_{11.3}O_{19}$) and CLC-M ($Ca_{0.5}La_{0.5}Co_{0.3}Fe_{10.1}O_a$, a≈19) by neutron diffraction and EXAFS measurements. Fig. 1 shows the one half of unit cell for Sr-M ($SrFe_{12}O_{19}$, space group: $P6_3/mmc$). The five different sublattices for the ferric ions are denoted using Wyckoff's notation as follows: 12k, 2a, $4f_2$ (octahedral sites), $4f_1$ (tetrahedral site) and 2b (bipyramidal site). In this study, we estimated the local structure on the assumption that cobalt ions simultaneously occupy some of the five ferric ion sites. It was suggested that cobalt ions are partitioned in the 2a, $4f_1$ and 12k sites in the ratio of 1:2:2 for SLC-M. Meanwhile, it was suggested that cobalt ions are partitioned in the 2a, $4f_1$ and 12k sites in the ratio of 2:6:2 for CLC-M.

Fig. 2 shows the X-ray absorption near edge structure (XANES) spectra and the XMCD spectra at the Fe *K*-edge for Sr-M, SLC-M and CLC-M. The ferric ions at the tetrahedral site (A site) of the spinel ferrite give a pre-edge peak around *E*≈7.11 keV in the XANES spectrum[6)]. The pre-edge peak is observed in the XANES spectra at the Fe *K*-edge for Sr-M, SLC-M and CLC-M. The M type ferrite has a ferrimagnetic structure, that is, eight ferric ions with the up-spin at 2a, 2b, 12k and four ferric ions with the down-spin at $4f_1$, $4f_2$ exist in a unit cell. The pre-edge peak originates from the ferric ions of the down spin at the tetrahedral site, $4f_1$. The intensity of the XMCD spectrum peak at the pre-edge peak is smaller for CLC-M than for Sr-M and SLC-M. This suggests that the contributions of the ferric ions in the down spin site to a magnetic moment decreases, suggesting that the ferric ions at the tetrahedral site $4f_1$ is replaced by more elements of a smaller or no magnetic moment for CLC-M compared to Sr-M and SLC-M.

## 3. Microstructural analysis of Ca-La-Co M-type sintered ferrite magnets by Cs-STEM[7)]

We investigated composition and microstructure at the vicinity of grain boundary by Cs-STEM for CLC-M sintered body. Table 1 shows EDX analysis results for multiple-junction phases of CLC-M sintered body with additives : (a) $CaCO_3$:0.0 mass%, $SiO_2$:0.34 mass%, (b) $CaCO_3$:1.25 mass%, $SiO_2$:0.68 mass%. It was confirmed that there are Ca-Si based oxides, which consists of Si, Ca, La and Fe, at multiple-junction phases of sintered body by adding only $SiO_2$ instead of both $CaCO_3$ and $SiO_2$ which are sintering aids for ferrite magnets. And then it was almost confirmed that the abundance ratio of Si, Ca, La and Fe at multiple-junction phases is 30：60：2：5.

Fig. 3 shows HAADF-STEM image on intergranular grain boundary for CLC-M sintered body with additives : $CaCO_3$:1.25 mass%, $SiO_2$:0.68 mass%. We found that the step-terrace structure of Ca-Si based oxides are formed at the surface of the M-type ferrite grain, and the maximum width of intergranular grain boundary is nearly equal to half the edge length along z-axis, which is 1.15 nm, of M-type ferrite unit cell. This suggests that M-type ferrite grains were magnetically isolated by the presence of Ca-Si based oxide phases at intergranular grain boundary.

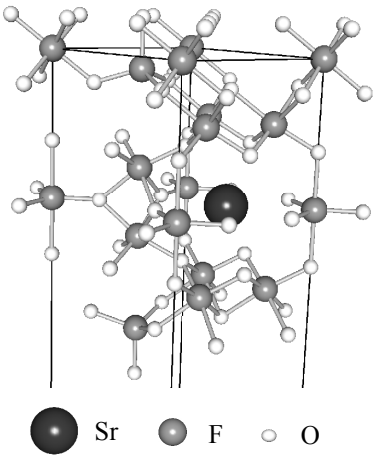


Fig.1 One half of unit cell of the Sr-M type hexaferrite ($SrFe_{12}O_{19}$, space group: $P6_3/mmc$).

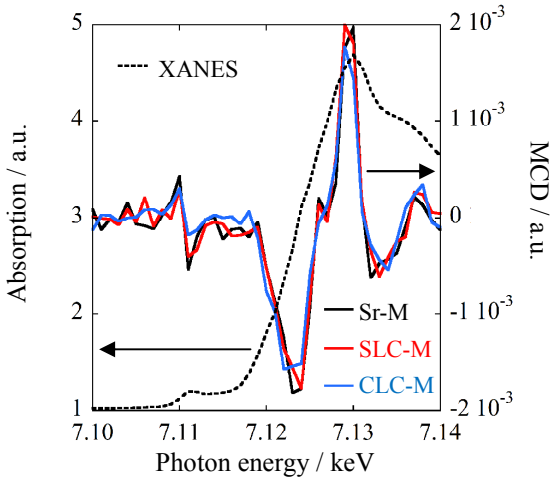


Fig. 2 The XANES and hard X-ray MCD spectra for the Sr-M and the La-Co substituted M type ferrite.

Table 1 EDX analysis results for multiple-junction phases of CLC-M sintered body with additives.

(a) $CaCO_3$:0.0 mass%, $SiO_2$:0.34 mass%

| | Si (at%) | Ca (at%) | La (at%) | Fe (at%) |
|---|---|---|---|---|
| 1 | 29.3 | 64.1 | 2.7 | 3.9 |
| 2 | 27.7 | 67.2 | 1.6 | 3.5 |
| 3 | 32.4 | 60.2 | 2.0 | 5.4 |
| 4 | 29.7 | 60.4 | 3.3 | 6.6 |
| 5 | 30.9 | 63.9 | 1.3 | 3.9 |
| Ave. | 30.0 | 63.1 | 2.2 | 4.7 |

(b) $CaCO_3$:1.25 mass%, $SiO_2$:0.68 mass%

| | Si (at%) | Ca (at%) | La (at%) | Fe (at%) |
|---|---|---|---|---|
| 1 | 30.2 | 63.5 | 1.2 | 5.1 |
| 2 | 30.9 | 62.0 | 1.5 | 5.6 |
| 3 | 30.7 | 63.3 | 1.7 | 4.3 |
| 4 | 30.1 | 62.2 | 1.9 | 5.8 |
| 5 | 31.7 | 60.5 | 1.1 | 6.7 |
| Ave. | 30.7 | 62.3 | 1.5 | 5.5 |

Fig. 3 HAADF-STEM image on intergranular grain boundary for CLC-M sintered body with additives. ($CaCO_3$:1.25 mass%, $SiO_2$:0.68 mass%)

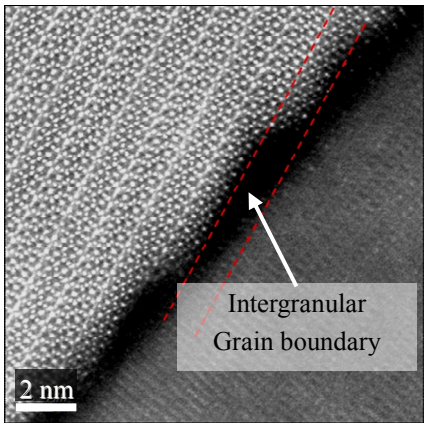


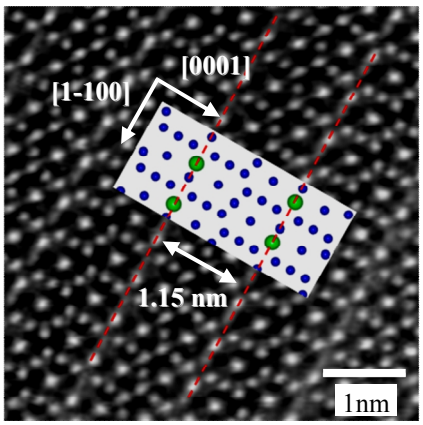


Reference

1) K. Iida, Y. Minachi, K. Masuzawa, J. Magn. Soc. Jpn., 23 (1999) 1093-1096.
2) H. Nishio, K. Iida, Y. Minachi, K. Masuzawa, M. Kawakami, H. Taguchi, J. Magn. Soc. Jpn., 23 (1999) 1097.
3) Y. Kobayashi, S. Hosokawa, E. Oda, S. Toyota, J. Jpn. Soc. Powder Powder Metallurgy, 55 (2008) 541.
4) Y. Kobayashi, E. Oda, T. Nishiuchi and T. Nakagawa, J. Ceram. Soc. Jpn., 119[4] (2011) 285.
5) Y. Kobayashi, E. Oda, T. Nakagawa and T. Nishiuchi, J. Jpn. Soc. Powder Powder Metallurgy, 63 (2016) 101.
6) N. Kawamura, Doctoral thesis, University of Okayama, Okayama, Japan, (1999) 88.
7) Y. Kobayashi, T. Kawata, submitted.

# Observations of Coercivity in RE-Fe-B Magnets in Pulsed Fields up to 30T

K. Nakahata[1], K Yamada[2], H. Shimoji[3] and M. Enokizono[4]
[1]Oita Advance Technical Academy, Oita 870-1141, Japan
[2]Saitama University, Saitama 338-8570, Japan
[3]Oita Pref. Industrial Research Institute, Oita 870-1117, Japan,
[4]Oita University, Oita 870-1192, Japan

The measurements of the coercivity (*Hc*) of magnets are very important to obtain the stored energies in magnets. However it is difficult to determine *Hc* as a function of the effective fields in samples with arbitrary shapes in pulsed fields. We tried to obtain the exact coercive force and the *M-H* curve in high pulsed magnetic fields up to 30T with long pulsed fields (e.g. half width of 80ms in $20T_{max}$) by using an induction method with a triple-fold pick-up coil [1]. In this experiment, the values of *Hc* were found much smaller than *10-20*% in the Nd-Fe-B and in Sm-Fe-B magnets which were supplied and announced ratings by a company. These errors might be caused by the sample insertion gap in between the sample and probe. These magnetic field configurations of samples with some insertion gaps of the pick-up coil were well simulated using JMAG and were well coincide with the experimental results. Fig. 1 shows the experimental results of $H_{eff}$ vs. $\mu_0 H$ for two samples of Nd-Fe-B. Table1 shows the discrepancies of the several parameters between the announced values and those in this study. Here it must be noted that we obtained the same samples with a sample maker and we prepared two types of samples which were cut along easy and hard axis, respectively. Therefore, to avoid errors, we prepared samples with the largest diameter up to the allowance to insert samples into the inner diameter of the pick -up coil (*10*mm$^{\Phi}$). The physical origin of this discrepancy is very plausible to consider the magnetic flux density at $B=\mu_0 H_{eff}+M$. In other words, at the coercive field (*Hc, M=0*), the effective fields as a function of the positions are uniform as described by $B= \mu_0 H_{eff} (=\mu_0 Hc)$. Therefore the voltages in the pick-up coil with its cross section are always larger than those of the samples by the insertion gap.

**References**

[1] K. Nakahata,B. Borkovsky, K. Yamada,T. Todaka, M. Enokizono, J. AEM,Vol.19,No2,pp207-212, ,2011

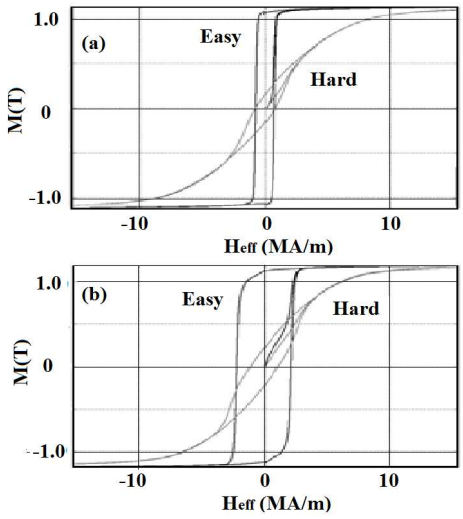


Fig.1 Experimental results of M-H curves of Nd-Fe-B magnets measured along Easy and Hard axes in pulsed fields

Table 1. Experimental results of typical samples

| **Nd-Fe-B(1)** | Easy | Hard | Easy(Catalog) |
|---|---|---|---|
| Mr (T) | 1.48 | 0.168 | 1.48 |
| $H_{cB}$(kA/m) | 867 | 91.1 | 1046 |
| $H_{cJ}$(kA/m) | 1024 | 607 | 875 |
| $(BH)_{Max}$ | 314 | 3.90 | 421 |

| **Nd-Fe-B(2)** | Easy | Hard | Easy(Catalog) |
|---|---|---|---|
| Mr (T) | 1.12 | 0.16 | 1.13 |
| $H_{cB}$(kA/m) | 697.2 | 92.3 | 835 - 915 |
| $H_{cJ}$(kA/m) | 2499 | 1051 | 2387 |
| $(BH)_{Max}$ | 197 | 3.76 | 240 |

| **Sm-Fe-B(c)** | Easy | Hard | Easy(Catalog) |
|---|---|---|---|
| Mr (T) | 1.07 | 0.16 | 1.08 |
| $H_{cB}$(kA/m) | 579 | 88.9 | 557 |
| $H_{cJ}$(kA/m) | 753 | 767 | 598 |
| $(BH)_{Max}$ | 174.8 | 3.48 | 215 |

# $Tb_2Fe_{14}B$/Fe コアシェル系のバルク単一粒子磁化反転 ～ Fe との交換結合による硬磁性化～

加藤宏朗，坂口麗美，板倉　賢*，小川大介，小池邦博，安藤康夫**（山形大，* 九州大，** 東北大）

Switching of bulk single particle in $Tb_2Fe_{14}B$/Fe core-shell system
– magnetic hardening by exchange coupling with Fe –

H. Kato, R. Sakaguchi, M. Itakura*, D. Ogawa, K.Koike and Y. Ando**
(Yamagata Univ., *Kyushu Univ., **Tohoku Univ.)

我々の研究グループでは，薄膜プロセスを用いて焼結磁石の主相と粒界相の界面状態を模したモデル界面を構築し，その界面状態と保磁力の関係を調べることで，ネオジム系焼結磁石の保磁力機構にアプローチしている．これまで，設計膜厚の制御によって粒子サイズを 300 nm から 50 nm まで系統的に変化させた $Nd_2Fe_{14}B$ 粒子を作製したところ，その保磁力が粒径減少に伴って系統的に増加することや，これらの試料に Nd 層や La 層を被覆して熱処理することで，保磁力が粒径に依らず増大する現象 [1, 2] 等を見出している．この結果は，保磁力増大に有用であるとされる「粒径減少」と「界面制御」という 2 つの要因は各々独立であり、両者は加算的に寄与することを示唆している．従って，$Nd_2Fe_{14}B$ バルク単結晶のように粒径が極端に大きな場合でも「適切な界面制御」がなされれば，反転核生成が抑制され保磁力発現の可能性があると考えられる．そこで本研究では，$Nd_2Fe_{14}B$ 系のバルク単結晶試料について，その表面状態と保磁力の関係を調べることで，ネオジム磁石の保磁力増大への指針を得ることを目的とした．今回は，$Nd_2Fe_{14}B$ よりも磁気異方性が大きく，表面状態の変化が保磁力へ顕著に影響すると期待される $Tb_2Fe_{14}B$ バルク単結晶を対象とし，その表面状態と保磁力の関係を系統的に調べた結果を主に報告する．

実験に使用した $Tb_2Fe_{14}B$ バルク単結晶は，浮遊帯溶融法で育成されたもので，X 線背面反射ラウエ法によってその結晶方位を決定し，種々のアスペクト比をもつ直方体形になるように切断・研磨した．直方体の各辺の長さは 0.3 mm ～ 1.5 mm である．各試料は，$Nd_2Fe_{14}B$ 型正方晶構造の (001) 面および (100) 面に平行な表面が最大面積になり，その法線方向が最短になるような板状に成形したものを，各々 (001) 試料および (100) 試料と命名した．単結晶試料の表面状態は多くの場合，空気中放置による「自然酸化状態」であるが，一部の試料については，超高真空スパッタ装置を用いて，到達真空度 $4.0\times10^{-6}$ Pa，Ar ガス圧 1.0 Pa，投入電力 20 W の条件で 4 時間，逆スパッタによるドライエッチングを行い，酸化被膜等の除去を試みた．この試料については，酸化防止層として in-situ で Mo 膜を 20 nm 成膜した．

系統的な実験によって，自然酸化状態の試料の容易軸方向における磁化曲線から，以下の結果を得た．

(1) *c* 面に平行な板状の $Tb_2Fe_{14}B$ (001) バルク単結晶では，減磁過程においてステップ的な磁化減少が見られた．

(2) 上記試料における磁化減少のステップ幅は，試料のアスペクト比に依存し，*c* 面の面積が減少し，*c* 軸方向の厚みが増大すると，系統的に増加することがわかった．

(3) *c* 軸に平行な細長い形状の $Tb_2Fe_{14}B$ (100) バルク単結晶は，角形比がほぼ 100％のスクエア型ヒステリシスを示し，その保磁力は，室温で 3 ~ 5 kOe の値をとることがわかった．

(4) これらの試料について TEM 観察を行ない，その表面状態を調べたところ，空気中に放置した自然表面をもつバルク単結晶 $Tb_2Fe_{14}B$ 試料では，その表面に 100 nm 以上の厚さを有する $\alpha$-Fe 相が存在することが確認

された．

上記 (4) の結果から，この試料は，mm サイズの $Tb_2Fe_{14}B$ コアが，数 100 nm 厚の $\alpha$-Fe シェルで囲まれた，コア・シェル構造を持っていることを示している．この $Tb_2Fe_{14}B$ コアに $\alpha$-Fe シェルが接していることで，$Tb_2Fe_{14}B$ 界面に Tb が露出している場合でも，Fe との交換結合によって異方性低下が抑制 [3] され，保磁力が発現している可能性がある．一方，$Tb_2Fe_{14}B$ コアと $\alpha$-Fe シェルの界面においては，我々がこれまで報告した $Nd_2Fe_{14}B$ / $\alpha$-Fe 系での交換結合状態 [4-6] と同様に，$Tb_2Fe_{14}B$ (001) / α-Fe 界面で正の交換結合，$Tb_2Fe_{14}B$ (100) / $\alpha$-Fe 界面で負の交換結合が成り立っていると推定 [7] される．以上のことから，一連の実験結果 (1)~(3) は，$Tb_2Fe_{14}B$ (100) / $\alpha$-Fe 界面での負の交換結合と，Fe が隣接することによる結晶場回復，及び垂直磁化をもつ板状磁性体の反磁場を考慮したコア・シェルモデル仮説で系統的に説明可能であることがわかった．

References


1) K. Koike, T. Kusano, D. Ogawa, K. Kobayashi, H. Kato, M. Oogane, T. Miyazaki, Y. Ando and M. Itakura, Nano. Res. Lett., (2016) 11:33.
2) K. Koike, H. Ishikawa, D. Ogawa, H. Kato, T. Miyazaki, Y. Ando, and M. Itakura, Coercivity enhancement in La coated Nd-Fe-B thin films, Physics Procedia, 75, (2015), 1294-1299.
3) R. Sasaki, D. Miura, and A. Sakuma, Appl. Phys. Exp., 8 (2015) 043004.
4) D. Ogawa, K. Koike, S. Mizukami, M. Oogane, Y. Ando, T. Miyazaki and H. Kato, J. Magn. Soc. Jpn., 36 (2012) 5.
5) D. Ogawa, K. Koike, S. Mizukami, T. Miyazaki, M. Oogane, Y. Ando, and H. Kato, J. Kor. Phys. Soc., 63 (2013) 489.
6) D. Ogawa, K. Koike, S. Mizukami, T. Miyazaki, M. Oogane, Y. Ando, and H. Kato, Appl. Phys. Lett., 107, (2015) 102406.
7) N. Umetsu, A. Sakuma, and Y. Toga, Phys. Rev. B 93 (2016) 014408.

# First principles study on effect of stabilizing element M in $NdFe_{11}M$

Yosuke Harashima[1,2], Kiyoyuki Terakura[3], Hiori Kino[3], Shoji Ishibashi[1], Takashi Miyake[1,2,3]
([1]AIST CD-FMat, [2]NIMS ESICMM, [3]NIMS CMI[2])

Recent experiment succeeded epitaxial growth of a film sample of $NdFe_{12}N$. The sample shows larger magnetization and stronger magnetocrystalline anisotropy than $Nd_2Fe_{14}B$ [1]. $NdFe_{12}N$ and its related materials can be expected as good candidates for the permanent magnet materials [1,2]. $NdFe_{12}N$ is synthesized from $NdFe_{12}$ by interstitial nitrogenation to enhance the magnetization and the magnetocrystalline anisotropy (see Ref [3] for the effect of nitrogenation). Even though the epitaxial growth of $NdFe_{12}$ is succeeded, synthesis of the bulk sample is still difficult. To stabilize the materials, third elements, ex.) Ti, have been used, but the magnetization is reduced by the substitution [4]. For the stabilizing elements, much stability with less amount of substitution and less reduction of the magnetization are required.

The purpose of this study is to find better stabilizing elements for $NdFe_{11}M$ in terms of the stability, the magnetization, and the magnetocrystalline anisotropy. We perform the first principles calculation of $NdFe_{11}M$ (M=Ti, V, Cr, Mn, Fe, Co, Ni, Cu, Zn) and estimate the stability, the magnetization, and the magnetocrystalline anisotropy.

The calculation is performed by using QMAS [5] based on the density functional theory and the projector augmented-wave method. The exchange-correlation energy functional is approximated by using the generalized gradient approximation. Nd-4f electrons are treated as open-core states. The magnetocrystalline anisotropy is estimated from the crystal field parameter $A_2^0$.

To estimate the stability of $NdFe_{11}M$, we calculate the formation energy by M substituted with Fe. The formation energies for Ti, V, Cr, Mn give negative values, and especially Ti stabilizes the alloy more than other elements. In experiments, these alloys are indeed observed and the amount of substitution of Ti is less than other elements. We found that Co, Ni, Zn also give negative formation energies, and that the stability of $NdFe_{11}Co$ are comparable to that of $NdFe_{11}Ti$. $NdFe_{11}Co$ has as large magnetization as $NdFe_{12}$. Nitrogenation enhances the magnetization of $NdFe_{11}Co$. For the magnetocrystalline anisotropy, nitrogenation enhances the crystal field parameter as well as $NdFe_{12}$ and $NdFe_{11}Ti$. This indicates that the uniaxial anisotropy is enhanced by nitrogenation.

As conclusion, Co is a good stabilizing element for $NdFe_{11}M$.

In our talk, we will also discuss the effect of Zr substitution.

Reference

1) Y. Hirayama, Y. K. Takahashi, S. Hirosawa, and K. Hono, Scr. Mater. **95**, 70 (2015).
2) S. Suzuki, T. Kuno, K. Urushibata, K. Kobayashi, N. Sakuma, K. Washio, M. Yano, A. Kato, and A. Manabe, J. Magn. Magn. Mater. **401**, 259 (2016).
3) Y. Harashima, K. Terakura, H. Kino, S. Ishibashi, and T. Miyake, Phys. Rev. B **92**, 184426 (2015).
4) T. Miyake, K. Terakura, Y. Harashima, H. Kino, and S. Ishibashi, J. Phys. Soc. Jpn. **83**, 043702 (2014).
5) http://qmas.jp

# Temperature-dependence of Nd magnetic moment in a $NdFe_{12}N_x$ thin film by X-ray magnetic circular dichroism

Y. Hirayama*, T. Nakamura**, Y K. Takahashi*, S. Hirosawa* and K. Hono*
(*ESICMM/NIMS, ** JASRI/SPring-8)

## BACKGROUND

The saturation magnetization, $M_s$, of $NdFe_{12}N$ compounds with $ThMn_{12}$ structure is expected to be a high $M_s$ because of a high concentration of Fe[1]. Recently, we successfully prepared the $NdFe_{12}N_x$ film with the $M_s$ of 1.66 ± 0.08 T at 300 K.[2] Moreover, the Curie temperature of $NdFe_{12}N_x$ was 150 °C higher than that of $Nd_2Fe_{14}B$. However, the $M_s$ and the anisotropy field, $H_A$, decays more rapidly as the temperature increase for $NdFe_{12}N_x$ compared with those of $Nd_2Fe_{14}B$ and $Sm_2Fe_{17}N_3$.[3] These trends of the $M_S$ and $H_A$ against temperature strongly depend on the strength of the indirect exchange coupling of Nd(4*f*)-Fe(3*d*) according to the *ab* initio-based calculation[4]. In order to investigate the origin of the trend of the $M_s$ against temperature, we measured the temperature dependency of the Nd magnetic moment by measuring temperature dependency of amplitude of the magnetic circular dichroism (MCD) signal from the Nd-$M_{IV-V}$ edge.

## EXPERIMENTAL

MgO(001)//W/$NdFe_{12}N_x$(50 nm)/W(2 nm) was prepared by co-sputtering system followed by ref.2. The XMCD measurement was performed at SPring-8 BL25SU by using electromagnet in the range between -1.9 and +1.9 T at 300, 200, 100 and 15 K.

## RESULT

The MCD spectrum was successfully obtained through W cap layer of 2 nm for Nd-$M_{IV-V}$ edge although the probing depth for this XMCD measurement is several nm. Figure (a) shows the hysteresis curves for Nd magnetic moment at various temperatures. Here, the vertical axis was normalized at the value at 15 K and 1.9 T. The magnetic moment of Nd decreases almost lineally with increasing temperature and 30 % of the Nd moment was missing at 300 K as shown in Fig. (b). This trend is different from the total magnetization of $NdFe_{12}N_x$, which is dominated by the Fe magnetic moments, indicating that the indirect Nd(4*f*)-Fe(3*d*) coupling might be relatively weak[4].

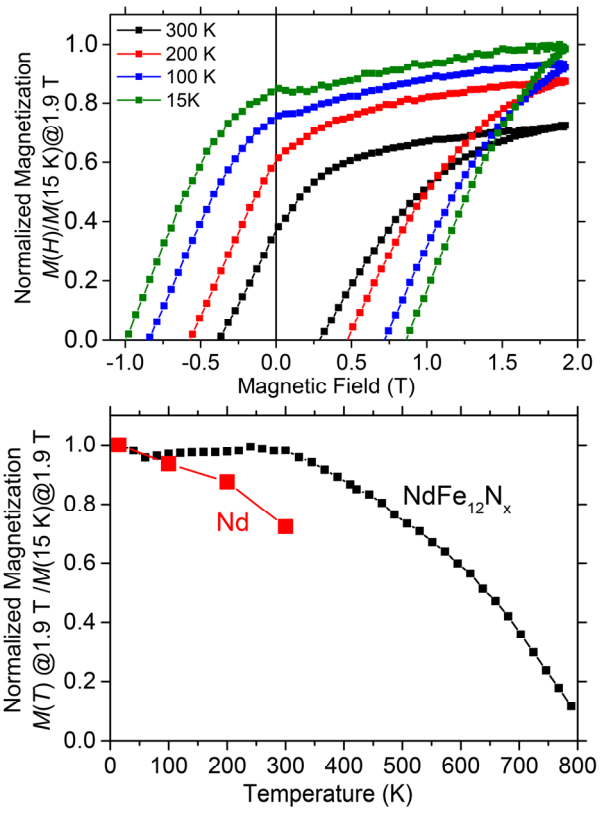


Fig (a) The magnetic hysteresis obtaining from Nd-$M_{IV, V}$ edge at various temperature of 300, 200, 100 and 15 K. (b)The temperature dependence of the Nd magnetic moment together with the total magnetic moment of $NdFe_{12}N_x$.

## REFFERENCE

1) T. Miyake *et al.*, *J. Phys. Soc. Jpn.* 83, 043702 (2014)
2) Y. Hirayama *et al.*, *Scripta Materialia* **95**, 70 (2015).
3) Y. Hirayama *et al.*, *JOM*, **67**, 1344 (2015).
4) M. Matsumoto *et al.*, *J. Appl. Phys*. **119**, 213901 (2016)

# 等方性 Nd–Fe–B 焼結磁石の高温その場中性子回折

斉藤耕太郎, 小野寛太, ステファヌス・ハルヨ *, 深川智機 **, 西内武司 **
(高エネルギー加速器研究機構, * 日本原子力研究開発機構, ** 日立金属（株）)

In-situ high temperature neutron diffraction study of isotropic Nd–Fe–B sintered magnet

K. Saito, K. Ono, Stefanus Harjo*, T. Fukagawa** and T. Nishiuchi**
(High Energy Accelerator Research Organization, *Japan Atomic Energy Agency, **Hitachi Metals, Ltd.

## 1　はじめに

高保磁力の Nd-Fe-B 焼結磁石を作るためには副相の制御が重要であり、焼結後に適切な温度・時間で熱処理することにより磁石の保磁力が向上することはよく知られている。熱処理条件や副相の分布に関してはすでに多くの顕微的研究が行われており、保磁力向上は $Nd_2Fe_{14}B$ 主相粒を包む副相の体積率や分布の熱処理による最適化であると考えられている [1,2]。しかし、試料表面の局所観察は多数報告されている一方で、磁石内部での副相の定量的な研究は我々の知る限り報告がない。本研究では、透過率が高くバルク試料全体の平均情報を得られる中性子を用いて、高温環境下で Nd–Fe–B 焼結磁石内部の副相がどう変化するかを検証した。

試料は 7mm 角、高さ 30 mm の直方体に切り出した 2 種類の等方性 Nd–Fe–B 焼結磁石（31.0Nd–1.0B–bal.Fe 及び Cu0.1% 添加試料）を用い、測定は MLF/J-PARC の工学材料回折装置 BL19 匠にて行った。室温から 900°C まで 0.7°C/min で昇温する間の連続測定を行い、ディラトメーターを用いて長軸方向の微小な長さの変化も同時に測定した。

## 2　結果および考察

両試料において同程度の強度の NdO (fcc) 及び $Nd_2O_3$ (A-type, hcp) の明瞭な回折ピークが観測され、Cu 0% 試料においてはいわゆる B rich 相と呼ばれる $Nd_5Fe_{18}B_{18}$ の回折ピークが観測された（Fig. 1）。リートベルト解析により求めた $Nd_2Fe_{14}B$、NdO、$Nd_2O_3$ の格子定数を Fig. 2 に示す。$Nd_2Fe_{14}B$ の格子定数は *a*, *c* 軸ともにキュリー温度以下で磁歪による特徴的な温度変化を示し、特に *c* 軸方向は Andreev らの報告した単結晶の格子定数とは異なる温度依存性を持つことが明らかになった [3]。NdO 及び $Nd_2O_3$ は主相のキュリー温度以上では温度に対して線形に変化する一方で、キュリー温度以下では主相の磁歪に影響を受けていることが明らかになった。これは副相が主相と格子結合していることを意味する。

主相の単位格子体積の三乗根と試料の長軸方向の長さの変化を比較した Fig. 3 からは、Cu 0% 試料では 750°C、Cu 0.1% 試料では 630°C 以上から試料長さが主相の単位胞の温度変化よりも過剰な増加を示すことがわかる。これは磁石内部の NdO、$Nd_2O_3$ 以外の副相、おそらくは dhcp 構造の Nd が溶解するためと考えられる。

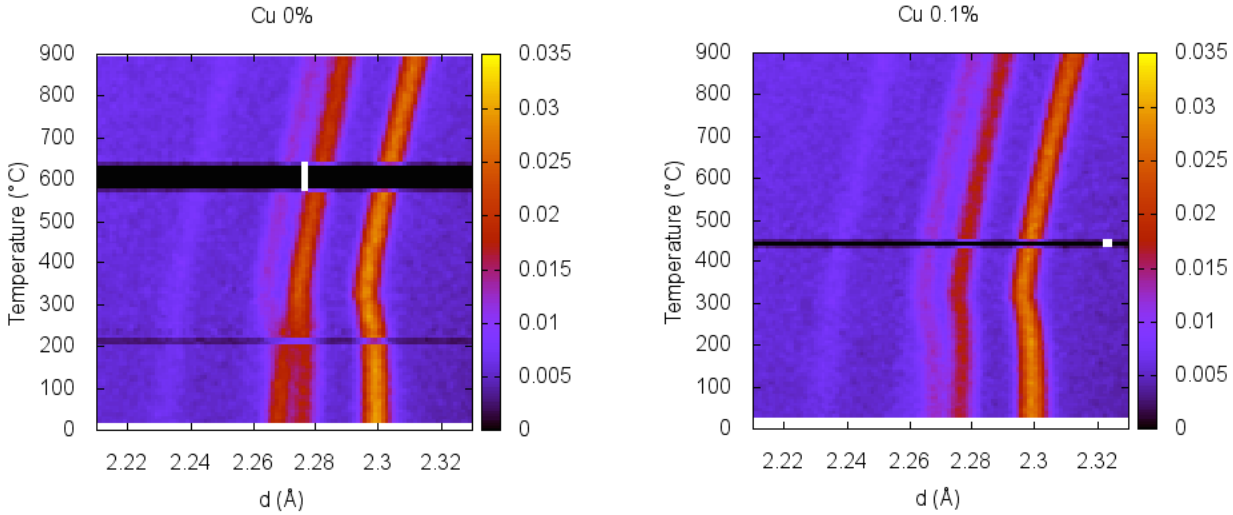


**Fig. 1**　B rich 相の回折ピーク

## References

1) R. Ramesh, J. K. Chen, and G. Thomas: *J. Appl. Phys.*, **61**, 2993 (1987).
2) T. Fukagawa and S. Hirosawa: *J. Appl. Phys.*, **104**, 013911 (2008).
3) A. V. Andreev, A. V. Deryagin, S. M. Zadvorkin, and S. V. Terent'ev: *Sov. Phys. Solid State*, **27** 987 (1985).

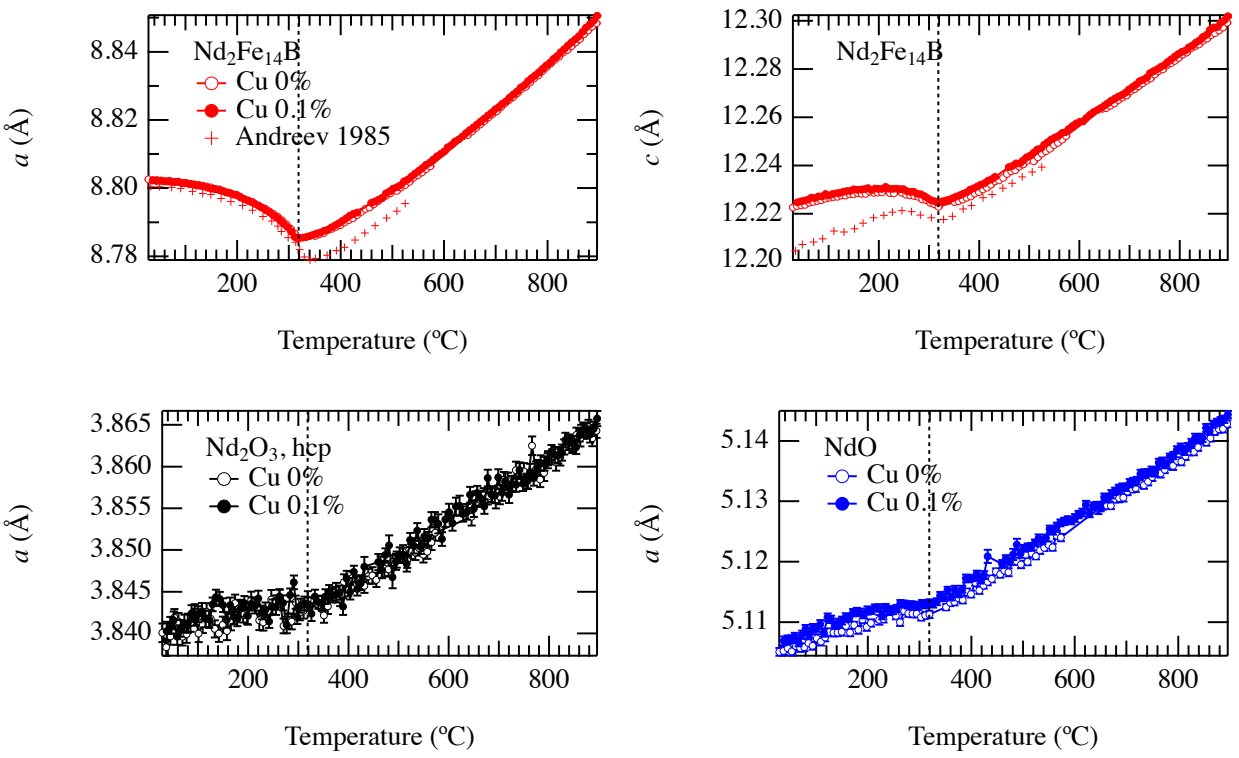


**Fig. 2** $Nd_2Fe_{14}B$、NdO、$Nd_2O_3$ の格子定数の温度変化

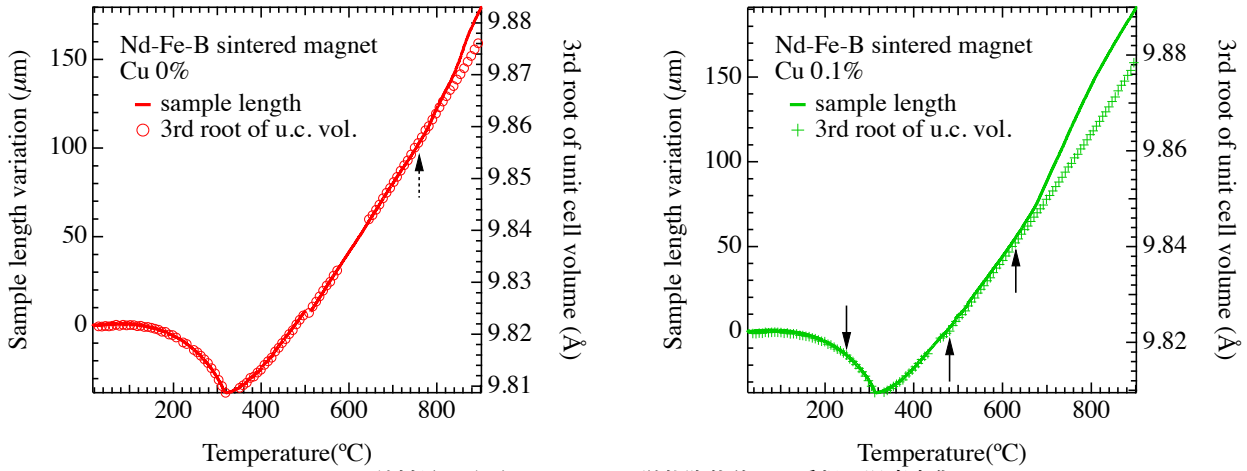


**Fig. 3** 試料長さ及び $Nd_2Fe_{14}B$ の単位胞体積の三乗根の温度変化

# Preparation of Rare-earth-saved hard magnetic materials

Masashi Matsuura, Nobuki Tezuka, and Satoshi Sugimoto
(Department of Materials Science, Graduate School of Engineering,
Tohoku University, Sendai 980-8579, Japan)

Rare-earth magnets are used in numerous devices and are essential materials. However, rare-earth elements, especially heavy rare-earth elements, are limited natural resources; therefore, it is important to develop rare-earth-free permanent magnets. Recently, developing rare-earth-free hard magnetic materials has been performed by using tins films, nano-powders, and non-equilibrium process. Some research have focused on α"-$Fe_{16}N_2$[1,2], $L1_0$-FeNi[3-5], and Mn alloy[6,7] showing relatively high magnetic anisotropy. Although Mn-based compounds show low saturation magnetization, some Mn-based compounds show high corecivity because of high crystalline anisotropy. Our group reported that Mn-Sn-N and Mn-Sn-Co-N alloys[8] exhibit high coercivity more than 800 $kAm^{-1}$ without rear-earth elements. High performance permanent magnets must have the large coercivity, therefore revelation of cause of high coercivity has possibility of important clue for development of new type magnets.

FeCo alloys are also candidates for rare-earth-free permanent magnets because they exhibit high saturation magnetization. FeCo alloys, which have a stable cubic structure phase, can show high magnetocrystalline anisotropy when the unit cell is distorted tetragonally.[9,10] In these days, distorted FeCo film grown on Ir(001), Pd(001) or Rh(001) underlayer have been reported by several researchers[11-13]. Our group reported that Rh/FeCo-Ti-N thin film has perpendicular magnetic anisotropy derived from lattice distortion at the interface[14].

Our group have also preparing nano-particles for high coericivity, and shows high coercive Mn-Bi and Fe nano-particles. Then, I introduce our recent research about rare-earth free hard magnetic materials. Topics are shown as follows;

- High coercive Mn-Sn-Co-N alloy

$Mn_{82.5}Sn_{10}Co_{7.5}$ (at%) alloy was annealed at 900 °C (high-temperature annealing) and subsequently annealed at 400-700 °C (low-temperature annealing) under $N_2$ gas atmosphere. The coercivity strongly depended on the low-temperature annealing and reached a maximum of 1270 $kAm^{-1}$ for annealing at 500 °C (Fig. 1). The alloy consists of two phases of perovskite-type Mn-N and β-Mn phases, and there are many twins and stacking faults in the perovskite-type phase. In addition, Co and Sn enriched at the twin interfaces. These results indicate that the magnetic anisotropy could change at twins, and the twins could play as a pinning site of domain wall motion for Mn-Sn-Co-N alloy.

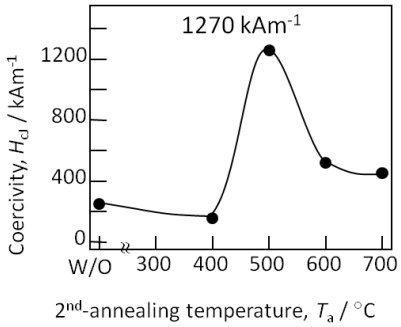


Fig. 1 2nd-annealing temperature dependence of coercivity of Mn-Sn-Co nitrided alloy.

- FeCo-Ti-N anisotropic films

FeCo-Ti-N thin films with the thickness ($t$) of 23~62 nm deposited on Rh buffer layer. The FeCo-Ti-N film shows relatively high anisotropy constant ($K_u$) of 0.98 $MJm^{-3}$ for t=23 nm (Fig. 2), and the value is 0.46 $MJm^{-3}$ for t=64 nm. Addition of Ti and N into FeCo layer improves lattice distortion of the lattice and it also improved the $K_u$.

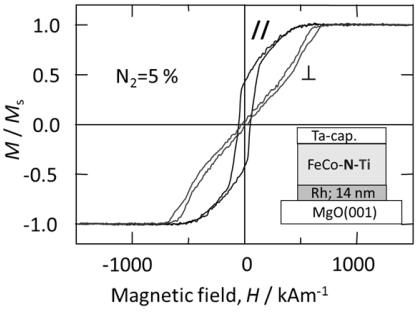


Fig. 2 Hysteresis loops measured with the external field perpendicular to the plane (⊥) and in-plane (//) directions for the FeCo-Ti-N films prepared with 5% $N_2$ gas.

- Mn-Bi and FeCo-based nano-particles with relatively high coercivity

High coercivity Mn-Bi nano-powder are obtained by Hydrogen-Plasma-Metal-Reaction (HPMR) process. The coercivity is 1090 $kAm^{-1}$, and $(BH)_{max}$ reached to 105 $kJm^{-3}$ [15]. The $(BH)_{max}$ is highest value for Mn-Bi. The HPMR process can prepare Fe-based nano-particles, and FeCo nano-particles shows relatively high coercivity over 90 $kAm^{-1}$.

Reference
1) T.K. Kim and M. Takahashi, Appl. Phys, Lett., **20** (1972) 492.
2) M. Komuro, Y. Kozono, M. Hanazono and Y. Sugita, J. Appl. Phys., **67** (1990) 5126.
3) L. Néel, J. Pauleve, R. Pauthenet, J. Langier, and D. Dauteppe, J. Appl. Phys., **35** (1964) 873 (1964).
4) J. Paulevé, A. Chamberod, K. Krebs, and A. Bourret, J. Appl. Phys., **39** (1968) 989.
5) A. Makino, P. Sharma, K. sato, A. Takeuchi, Y. Zhang, and K. Takenaka, Scientific Reports, **5** (2015) 16627.
6) F. Wu, S. Mizukami, D. Watanabe, H. Naganuma, M. Oogane, Y. Ando, and T. Miyazaki, Applied Physics Letters, **94** (2009) 122503 1-3.
7) H. Kurt, N. Baadji, K. Rode, M. Venkatesan, P. Stamenov, S. Sanvito, and J. M. D. Coey, Applied Physics Letters, **101** (2012) 132410 1-3.
8) K. Isogai, K. Shinaji, T. Mase, M. Matuura, N. Tezuka, and S. Sugimoto, Mater. Trans., **54** (2013) 1236.
9) T. Burkert, L. Nordström, O. Eriksson, and O. Heinonen, Phys. Rev. Lett., **93** (2004) 027203.
10) Y. Kota and A. Sakuma, Appl. Phys. Exp., **5** (2012) 113002.
11) F. Luo, X.L. Fu, A. Winkelmann, and M. Przybylski, Appl. Phys. Lett., **91** (2007) 262512.
12) B. Lao, J. Won, and M. Sahashi, IEEE Trans. Magn., **50** (2014) 2008704.
13) F. Yildiz, M. Przybylski, and J. Kirschner, J. Appl. Phys., **105** (2009) 07C312.
14) M. Matsuura, N. Tezuka, and S. Sugimoto, J. Appl. Phys., **117** (2015) 17A738.
15) K. Isogai, M. Matsuura, N. Tezuka, and S. Sugimoto, Mater. Trans., **54** (2013) 1673.

# Fabrication of tetragonal FeCo based alloy films with uniaxial magnetic anisotropy to develop an innovative permanent magnet

S. Ishio and T. Hasegawa

Department of Materials Science, Akita University, Japan

Based on the first principles calculation, tetragonal distorted FeCo alloy has large uniaxial anisotropy energy $K_{u1}$ and high saturation magnetization $M_s$, which is the most desirable feature for innovative permanent magnets [1,2]. In fact, the epitaxial tetragonal FeCo films with c/a~1.2 prepared on Rh buffer layer shows $K_{u1}$ larger than 1.5x10$^7$ erg/cm$^3$ [3,4]. FeCo-Al forms a B2 ordered phase in a wide composition range and is expected to enhance $K_{u1}$ through a B2 ordering and a huge magneto-elastic interaction [5]. In this study, the tetragonal $(Fe_{1-x}Co_x)_{1-y}M_y$ (x:0~1, y:0~0.2, M:Al, Ga etc) films are prepared on Rh buffer layer, and the uniaxial magnetic anisotropy is studied.

$(Fe_{0.5}Co_{0.2})_{0.9}M_{0.1}$(2~20nm)/Rh (20 nm)/MgO(100) and $Fe_{0.5}Co_{0.5}$(2~20nm)/Rh (20 nm)/ MgO(100) films were prepared in a high vacuum multiple dc-sputtering system with a base pressure lower than 1×10$^{-6}$ Pa. Rh thin film was first sputtered on the MgO (100) substrate at 300 °C. Then, after decreasing the temperature to 200 °C, FeCoM films were epitaxially grown on the Rh layer. Finally, $SiO_2$ was sputtered as a capping layer to prevent oxidation. The film structure was analyzed by in-plane and out-of-plane XRD. Magnetic properties were measured by VSM, Polar-Kerr measurements and torque magnetometer.

The values of $K_{u1}$ for $(Fe_{0.5}Co_{0.2})_{0.9}Al_{0.1}$ and $Fe_{0.5}Co_{0.5}$ films are plotted in Fig.1 as function of film thickness. These data are re-plotted as a function of the lattice distortion *c/a* in Fig.2, and its $K_{u1}$-*c/a* relation is understood by a tetragonal distortion [2]. $(Fe_{0.5}Co_{0.2})_{0.9}Al_{0.1}$ exhibits a maximum (2.1x10$^7$ erg/cm$^3$) around *c/a*~1.2. A coercivity *Hc* over 10 kOe is calculated from the single domain theory and, in fact, the coercivity of 3-7 kOe was observed in dot patterns with less than 100 nm in diameter. With taking account of *Ms*~1500 emu/cm$^3$, the tetragonal FeCo based alloy is one of the most probable candidates to develop an innovative permanent magnet with 60 MGOe. The results for other M metals will be introduced in the conference.

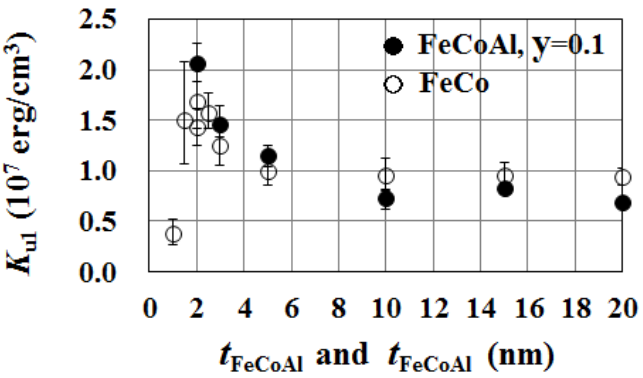


Fig.1　$K_{u1}$ as a function of film thickness for $(Fe_{0.5}Co_{0.5})_{0.9}Al_{0.1}$ and $Fe_{0.5}Co_{0.5}$ films.

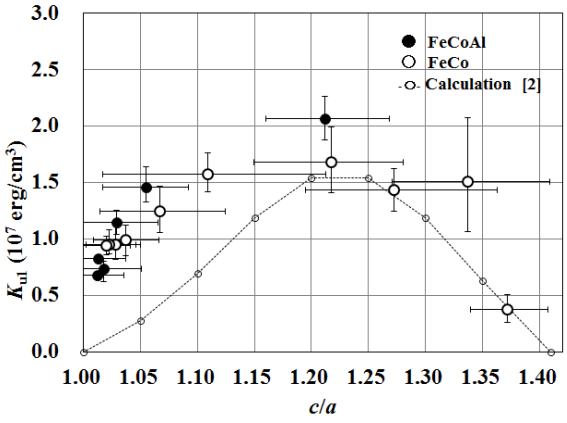


Fig.2　$K_{u1}$ as a function of *c/a* for $(Fe_{0.5}Co_{0.5})_{0.9}Al_{0.1}$ and $Fe_{0.5}Co_{0.5}$ films.

References

1) T. Burkert et al., *Phys. Rev. Lett. 93* (2004) 027203.
2) Y. Kota et al., *Appl. Phys. Express* 5 (2012) 113002.
3) H. Oomiya1 et al., *J. Phys*. 48 (2015) 475003.
4) B. Lao et al., IEEE Trans. Magn. 50 (2014) 2008704.
5) A. E. Clark et al., *IEEE Trans. Magn.* 36 (2000) 3238.

# Artificial fabrication and characterization of $L1_0$-FeNi thin films for rare-earth-free permanent magnets

M. Mizuguchi, T. Kojima, T. Y. Tashiro and K. Takanashi
Institute for Materials Research, Tohoku University, Sendai 980-8577, Japan

Large uniaxial magnetic anisotropy materials are extremely promising for the application to rare-earth-free permanent magnets. As one of the materials, $L1_0$-ordered FeNi alloy is attracting attention because it reveals large $K_u$ (uniaxial magnetic anisotropy energy) value in bulk[1]. However, it is difficult to obtain the $L1_0$ phase by conventional techniques because the order-disorder transformation temperature of $L1_0$-FeNi is too low (320 ˚C) and the migration of atoms is not fully promoted to form the ordered phase. From this reason, the artificial fabrication of $L1_0$-FeNi films from seems to be one of the scarce solutions to realize this material. In this study, we successfully obtained $L1_0$-FeNi thin films with a large $K_u$ by alternate monatomic layer deposition using molecular beam epitaxy (MBE)[2-8]. FeNi films including $L1_0$ phase were also fabricated by sputtering and post-annealing[9]. Structural and magnetic properties were systematically investigated for FeNi thin films, and clarified the origin of the large magnetic anisotropy in $L1_0$-FeNi.

FeNi films were fabricated by MBE employing an alternative monatomic deposition of Fe and Ni layers on several underlayers. They were fabricated also by sputtering on a MgO(001) substrate and subsequent rapid thermal annealing (RTA). Structural properties were investigated by X-ray diffraction (XRD) using synchrotron radiation and transmission electron microscope observation. Magnetic properties were characterized by a superconducting quantum interference device or a vibrating sample magnetometer.

$K_u$ of FeNi this film fabricated by MBE was evaluated to be about 0.7 MJ/m$^3$ from the magnetization curves, and it is confirmed that large magnetic anisotropy is induced by the formation of $L1_0$ type FeNi structure. The relationship between $K_u$ and chemical order parameter ($S$), which was estimated from XRD measurements, was investigated. $K_u$ was roughly proportional to $S$, indicating clear correlation between $K_u$ and $S$ as shown in Fig. 1. On the other hand, XRD patterns of FeNi films fabricated by sputtering drastically changed depending on the condition of RTA. Magnetization curves also changed with the annealing temperature and the annealing time, which implied the successful formation of $L1_0$-FeNi. In addition, the enhancement of coercivity ($H_{c\perp}$) and remanent magnetization ($M_{r\perp}/M_S$) with $S$ was observed associated with the appearance of $L1_0$ phase as shown in Fig. 2. The effect of the other-element-addition for FeNi on crystallographic and magnetic properties was also investigated for both MBE and sputtered FeNi films, and enhancement of $S$ or increase of the order-disorder transformation temperature was clarified.

The part of this work was supported by the Elements Strategy Initiative Project under the auspice of MEXT.

Reference

1) J. Paulevé *et al*., J. Appl. Phys., **39** (1986) 989.
2) T. Shima *et al*., J. Magn. Magn. Mater., **310** (2007) 2213.
3) M. Mizuguchi *et al*., J. Appl. Phys., **107** (2010) 09A716.
4) M. Mizuguchi *et al*., J. Magn. Soc. Jpn., **35** (2011) 370.
5) T. Kojima *et al*., Jpn. J. Appl. Phys., **51**(2012) 010204.
6) T. Kojima *et al*., J. Phys.: Conden. Matter, **26** (2014) 064207.
7) T. Kojima *et al.*, J. Phys. D: Appl. Phys., **47** (2014) 425001.
8) T. Kojima *et al.*, Thin Solid Films, **47** (2016) 348.
9) T. K. Tashiro *et al.*, J. Appl. Phys., **117** (2015) 17E309.

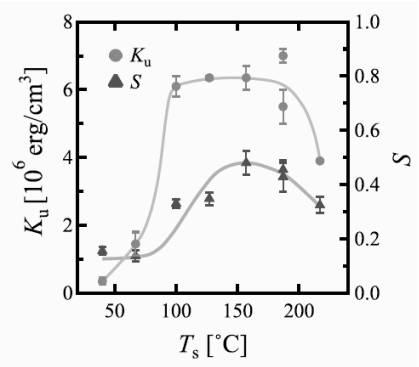


Fig. 1 Growth temperature ($T_s$) dependence of $K_u$ and $S$ [5].

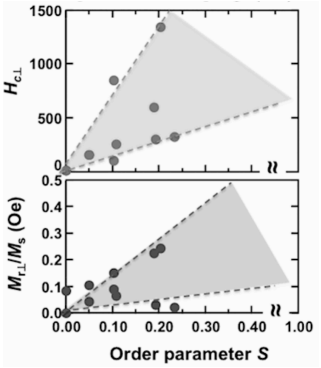


Fig. 2 $S$ dependence of $H_{c\perp}$ and $M_{r\perp}/M_S$.

# A Theoretical Approach to Synthesize $L1_0$ type FeNi Alloy Powder

Y. Hayashi[1], S. Goto[1], E. Watanabe[1], H. Kura[1], H. Yanagihara[2], E. Kita[3], M. Mizuguchi[4], K. Takanashi[4]
[1]Research Laboratories, DENSO CORPORATION, Aichi 470-0111, Japan
[2]Institute of Applied Physics, University of Tsukuba, Ibaraki 305-8573, Japan
[3]National Institute of Technology, Ibaraki College, Ibaraki 312-8508, Japan
[4]Institute for Materials Research, Tohoku University, Sendai 980-8577, Japan

$L1_0$ type FeNi alloy ($L1_0$ FeNi) is a potential candidate for a rare-earth free magnet. However its synthesis is very difficult as it shows an order-disorder transition temperature at 320°C. Various synthesis routes such as neutron irradiation[1)], alternate monoatomic layer deposition[2)] and chloride complex reduction[3)] have been investigated, but industrial synthesis has never been achieved. In this paper, a new route to synthesize $L1_0$ FeNi by nitriding and denitriding of the disordered alloy is presented.

The nitrogen in iron nitrides is interstitially located in the lattice and weakly interacts with metals. Nitrogen tends to coordinate around iron atoms since its affinity to iron is stronger than that to nickel. FeNiN, formed by the nitriding of disordered FeNi in a rapid stream of ammonia[4)], has an FeN/Ni alternation layer structure. The coordination of metal atoms to FeNiN is similar to that in $L1_0$ FeNi. Therefore it is expected that $L1_0$ FeNi can be synthesized by topotactic denitriding.

Dynamic simulations were performed by a combination of molecular dynamics (MD) and Monte Carlo (MC) methods. MD calculations were carried out using the free calculation code “LAMMPS”. The embedded atom model (EAM) potential was employed between metals, and the Lenard Jones (LJ) potential was applied between the metal and nitrogen. Results shown in Fig. 1. (a), (b) and (c) demonstrate nitriding, denitriding and the diffusion path of nitrogen, respectively. Iron and nickel were ordered in nitriding, and remained ordered in the denitriding process. In nitriding, the corner positions were ordered when the nitrogen/metal ratio was around 1/4. The face-center positions were ordered when the ratio was above 1/4. Nitrogen diffused randomly in nitriding, but it diffused along an iron layer during denitriding. This may be the reason why iron and nickel do not become disordered in the denitriding process.

This work was supported by the NEDO project “Developing high-performance magnetic materials in pursuit of high-efficiency motors”.

Reference

1) L. Neel et al., J. Appl. Phys., 35(1964) 873.
2) M. Mizuguchi et al., J. Magn. Soc. Jpn., 35(2011) 370.
3) Y. Hayashi et al., J. Magn. Soc. Jpn., 37(2013) 198.
4) R. J. Arnott et al., J. Phys. Chem. Solids Pergamon Press 15(1960) 152.

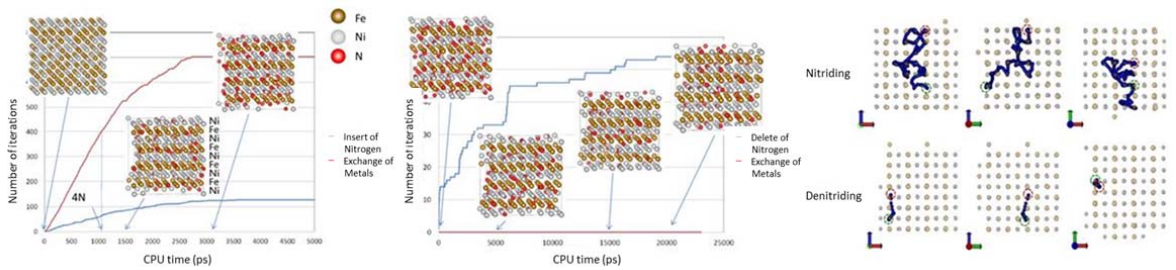


(a)Nitriding (b)Denitriding (c)Diffusion Path of Nitrogen

Fig. 1 Dynamic Simulations of Nitriding and Denitriding

# A New Route to Synthesize $L1_0$-type FeNi Alloy Powder

S. Goto[1], Y. Hayashi[1], E. Watanabe[1], H. Kura[1], H. Yanagihara[2], M. Mizuguchi[3], K. Takanashi[3], E. Kita[4]
[1]Research Laboratories, DENSO CORPORATION, Aichi 470-0111, Japan
[2]Institute of Applied Physics University of Tsukuba, Ibaraki 305-8573, Japan
[3]Institute for Materials Research, Tohoku University, Sendai 980-8577, Japan
[4]National Institute of Technology, Ibaraki College, Ibaraki 312-8508, Japan

$L1_0$-FeNi is a potential candidate for use in high performance magnets free of rare earth elements because of their high magnetic anisotropy. Various synthesis processes such as neutron irradiation[1)], alternate monoatomic layer deposition[2)] and chloride complex reduction[3)] have been carried out. However, a technique for obtaining a large content of this material has not yet succeeded. In this paper, we propose a route of large scale synthesis of $L1_0$-FeNi alloy in powder form by successive nitriding and denitriding of FeNi alloys.

We first optimized the nitriding conditions of FeNi alloy powders such as the process temperature, flow rate of $NH_3$ gas, and so on. Then a denitriding technique was developed to obtain $L1_0$-FeNi alloys by hydrogen gas treatment. In order to characterize the nitride and the reduced alloys, transmission electron microscope (TEM), scanning electron microscope combined with energy dispersive x-ray spectroscope (SEM-EDS) and x-ray diffraction (XRD) were employed. We also performed magnetization measurements at room temperature.

XRD results indicate coexistence of $(Fe,Ni)_2N$ as the main phase with $(Fe,Ni)_4N$ as the second phase (Fig.1). We also found that the iron and nickel atom positions of the $(Fe,Ni)_2N$ alloy are almost ordered. The estimated volume of the $(Fe,Ni)_2N$ phase was at least 85%. The denitrided FeNi alloy was mainly composed of the ordered phase of $L1_0$. We observed a correlation between the two order parameters of the FeNi nitrided alloy and the FeNi denitrided alloy. The order parameter and the magnetic coercivity of the $L1_0$-FeNi compound were $S$ = 0.67 and $H_c$ = 815 Oe, respectively (Fig.2).

This work was supported by the NEDO project “Developing high-performance magnetic materials in pursuit of high-efficiency motors.”

Reference

1) L. Neel et al., J. Appl. Phys., 35(1964) 873.
2) M. Mizuguchi et al., J. Magn. Soc. Jpn., 35(2011) 370.
3) Y. Hayashi et al., J. Magn. Soc. Jpn., 37(2013) 198.

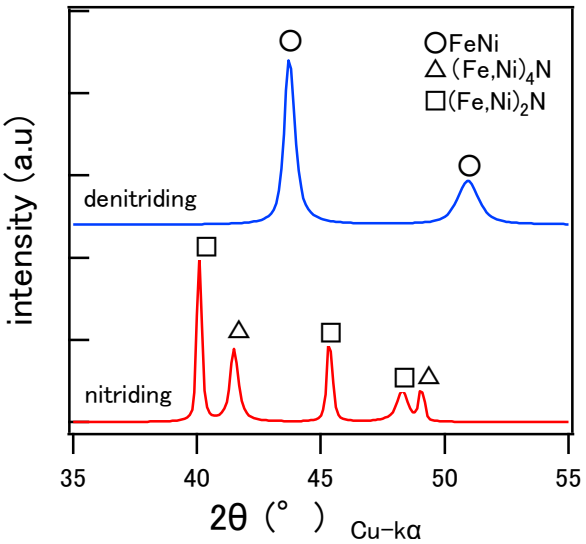


Fig1. Experimental x-ray diffraction patterns of the nitride FeNi (lower) and $L1_0$ phase (upper)

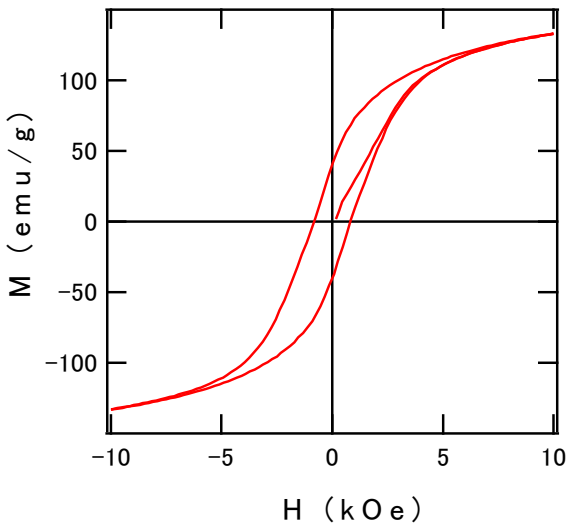


Fig.2 Magnetization curve at room temperature for a $L1_0$-FeNi powder

# d-HDDR 処理を施した Nd-Fe-B 磁石粉末の微細組織と異方性の関係

山崎理央[1,2]，堀川高志[2,3]，三嶋千里[2,3]，松浦昌志[1]，手束展規[1]，杉本諭[1]
（[1]東北大学，[2]愛知製鋼（株），[3]MagHEM）

Relationship between microstructure and anisotropy of Nd-Fe-B magnetic powder prepared by d-HDDR

M. Yamazaki[1,2], T. Horikawa[2,3], C. Mishima[2,3], M. Matsuura[1], N. Tezuka[1], and S. Sugimoto[1]
([1]Tohoku Univ., [2]Aichi Steel Corporation, [3]MagHEM)

## 諸言

Nd-Fe-B 系合金を高温下の水素中で不均化させ，その後，減圧下で水素を除去（脱水素）して再結合させる HDDR（hydrogen disproportionation desorption recombination）処理によって，組織が微細化し，高保磁力が得られる．また，不均化時の水素分圧と温度を適切に制御（d-HDDR 処理）することで，$Nd_2Fe_{14}B$ の結晶方位が揃った異方性粉末が得られることが知られている[1,2]．しかし，その異方化の起源については諸説あり，未だ明らかではない．そこで本研究では，不均化処理後にみられる Fe と $NdH_{2+x}$ からなるラメラ状組織に着目し，磁気特性と組織変化の関係を調べた．

## 実験方法

$Nd_{12.5}Fe_{bal}Ga_{0.3}Nb_{0.2}B_{6.2}$(at.%)組成のインゴットを水素解砕し，粉末粒径を 53~106 μm に分級した．この原料粉末を 30 kPa の水素雰囲気下で 820 °C, 1 min ~ 30 hr 保持（不均化処理）し，その後温度を保持したまま減圧して脱水素することで d-HDDR 処理した．なお，不均化処理後の組織を観察するため，水素雰囲気下で高温保持後，脱水素せずにそのまま冷却した試料（不均化試料）も作製した．得られた粉末の組織は，走査型電子顕微鏡（SEM）で観察，磁気特性は試料振動型磁力計（VSM）を用いて測定した．

## 実験結果

d-HDDR 処理後の異方化度の不均化処理時間依存性を調べた結果，不均化処理時間が長くなるにつれて，異方化度は低下する傾向がみられた．Fig. 1(a)に，不均化処理時間 1 hr で d-HDDR 処理した試料の SEM 像を示したが，0.6~1.4 μm 程度の粗大な結晶粒と，<500 nm 程度の微細な結晶粒が混在していた．この粗大な結晶粒は，不均化処理時間が長くなるにつれて減少する傾向を示した．そこで，不均化処理のみの試料の組織観察を行った．Fig. 1(b)に，1 hr 不均化処理後の組織を示したが，球状の結晶粒に加え，微細な二相からなるラメラ状の組織が混在していた．このラメラ状組織の領域は，0.6~1.4 μm 程度と，d-HDDR 処理後の粗大な結晶粒と同等であった．さらにこのラメラ状組織は，不均化処理時間が長くなるにつれて減少する傾向がみられた．以上の結果から，d-HDDR 処理に伴う異方化の要因として，ラメラ状組織が寄与している可能性が示された．

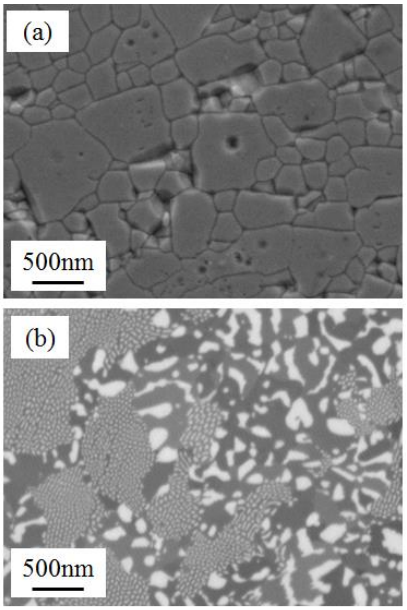


Fig. 1. (a) SE image of a particle of powder after d-HDDR, and (b) BSE image of a particle of powder after disproportionation. Both powders were treated for an hour at disproportionation treatment stage.

謝辞: 本研究は，国立研究開発法人新エネルギー・産業技術総合開発機構（NEDO）の委託事業「未来開拓研究プログラム／次世代自動車向け高効率モーター用磁性材料技術開発」の支援を受けて行われました．

## 参考文献

1) S. Sugimoto, *et al., J. Alloys Compd*. **293-295**, 862 (1999).
2) C. Mishima, *et al., IEEE Trans. Magn*. **37**, 2467 (2001).

# アークプラズマ蒸着法により作製した Sm-Fe-N/Zn 複合粉末の磁気特性

西島佑樹(院生)，松浦昌志，手束展規，杉本諭
（東北大学）

Magnetic properties of Sm-Fe-N/Zn powders prepared by arc plasma deposition

Yuki Nishijima, Masashi Matsuura, Nobuki Tezuka, Satoshi Sugimoto
(Tohoku University)

## 緒言

高い飽和磁化，異方性磁場，ならびにキュリー温度を有する $Sm_2Fe_{17}N_3$ 化合物を主相とする Sm-Fe-N 系 Zn ボンド磁石は高耐熱ボンド磁石としての利用が期待されている．高保磁力で高$(BH)_{max}$な Sm-Fe-N 系 Zn ボンド磁石を作製するためには，原料となる Sm-Fe-N 系粉末と Zn 粉末を均一に混合する必要があり，ボールミルなどによる機械的な混合方法が用いられている．更なる Zn の高分散化を実現するためには，Sm-Fe-N/Zn 複合粉末の作製が有効と考えられ，その手法として，スパッタリング法やアークプラズマ蒸着法が注目されている．本研究では，アークプラズマ蒸着法にて Sm-Fe-N 系粉末上に Zn 蒸着した Sm-Fe-N 複合粉末を作製し，熱処理に伴う磁気特性および組織変化を調べた．さらに，同粉末を圧粉して熱処理したときの磁気特性も調べた．

## 実験方法

アークプラズマ蒸着法を用い，$10^{-4}$ Pa 台の真空下，放電電圧 150 V，放電回数 20000 shots の条件で，Sm-Fe-N 系粉末(1.5 g)に Zn を蒸着した．また，比較のため，Sm-Fe-N 系粉末に対し市販の Zn 粉末(<7 μm)を 5 wt.%加え，ボールミルで混合した粉末も作製した．これらの粉末を，Ar ガス雰囲気下で 450 ~ 500 ºC で 30 min 熱処理した．更に，上記 2 種類の粉末を 2.3 MA·m$^{-1}$ の磁場中，200 MPa の圧力でのプレスにて圧粉体を作製し，Ar ガス雰囲気下で 475 ºC, 30 min 熱処理することにより Zn ボンド磁石を作製した．磁気特性は VSM または BH トレーサで，組成は XRF で測定し，組織は EDX を搭載した SEM で観察した．

## 実験結果

20000 shots のアークプラズマ蒸着により，Sm-Fe-N 系粉末への Zn 蒸着量は 5.1 wt.%であった．組織観察の結果，同量の Zn をボールミルで混合するよりも Zn の分散性が向上していることが分かった．Fig. 1 に，アークプラズマ蒸着法を用いて Zn を蒸着した Sm-Fe-N 系粉末および，ボールミルで Zn 粉末を混合した Sm-Fe-N 系粉末より作製した Zn ボンド磁石の減磁曲線を示した．Fig. 1 より，アークプラズマ蒸着法を用いて作製した Zn ボンド磁石の保磁力は，ボールミルで作製した Zn ボンド磁石よりも高い保磁力を示すことが分かった．

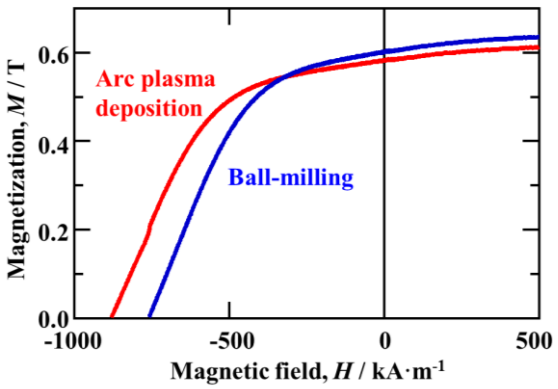


Fig. 1 Demagnetization curves of Zn-bonded Sm-Fe-N magnets prepared by arc plasma deposition and ball-milling

## 謝辞

本研究の一部は，国立研究開発法人新エネルギー·産業技術開発機構(NEDO)「未来開拓研究プロジェクト/次世代自動車向け高効率モータ用磁性材料技術開発プロジェクト」の支援の下，行われました．

# Micostructure-coercivity relationship in Nd-rich Ga-doped Nd-Fe-B sintered magnets

T.T. Sasaki, T. Ohkubo, Y. Takada**, T. Sato**, A. Kato***, Y. Kaneko**, K. Hono
(National Institute for Materials Science, **TOYOTA CENTRAL R&D LABS., INC,
***Toyota Motor Corporation)

Recent trend in coercivity improvement of Nd-Fe-B sintered magnet is to refine the grains size. However, magnetic alignment of fine particles of less than 3 μm is difficult in a large-scale industrial production process. Recently, Hasegawa et al. reported that a high coercivity ($\mu_0 H_c$) of 1.8 T can be achieved even for the sintered magnets with an average grain size of 6 μm. This opened up the realistic approach in achieving high coercivity in industrially viable Nd-Fe-B sintered magnets [1,2]. The alloy contains an excess amount of Nd and a small amount of Ga-dopant and the high coercivity was attributed to the formation of $Nd_6Fe_{13}Ga$ phase, and non-ferromagnetic grain boundary phase separating $Nd_2Fe_{14}B$ grains, both of which are rarely observed in standard commercial Nd-Fe-B sintered magnets. In this work, we analyzed the structure and chemical composition of the constituent phases at grain boundaries and triple junctions in the Nd-rich Ga-doped Nd-Fe-B sintered magnet annealed at various temperatures, and clarified the role of Ga on the substantial coercivity increase.

Two samples were used in this study. One is Nd-rich Ga-doped sintered magnet with the chemical composition of Fe-24.6Nd-7.87Pr-0.85B-0.13Cu-0.92Co-0.35Al-0.53Ga (wt.%), and the other is Ga-free magnet with the chemical composition of Fe-24.6Nd-7.87Pr-0.85B-0.13Cu-0.92Co-0.35Al (wt.%). Hereafter, these samples are denoted as Ga-doped sample and Ga-free sample, respectively. The sintered samples were post-sinter annealed at various temperatures for 1 h in a vacuum atmosphere. The microstructures of the samples were analyzed by scanning electron microscope (SEM, Carl-Zeiss Cross Beam 1540EsB), transmission electron microscope (TEM, FEI Titan G2 80-200).

Figure 1 shows the variations in the coercivity ($\mu_0 H_c$) as functions of post-sinter annealing temperature. Ga-doped samples exhibit higher coercivity compared to the Ga-free samples, and the temperature range to achieve high coercivity in the Ga-doped sample is much wider compared to the Ga-free sample. Figure 2 shows backscattered electron SEM images of as-sintered samples and the samples annealed at 480, 600 and 750°C. In all samples, Nd-rich phases are present at grain boundary triple junctions. The variation in the areal fraction of the $Nd_6Fe_{13}Ga$ phase is consistent with the change in coercivity. Thick non-ferromagnetic grain boundary phase is formed between neighboring $Nd_2Fe_{14}B$ grains in the samples annealed at 480 and 600°C. Therefore, the main reason for the substantial coercivity increase can be attributed to the formation of non-ferromagnetic grain boundary phase. Based on these results, the effect of $Nd_6Fe_{13}Ga$ phase on coercivity will be discussed.

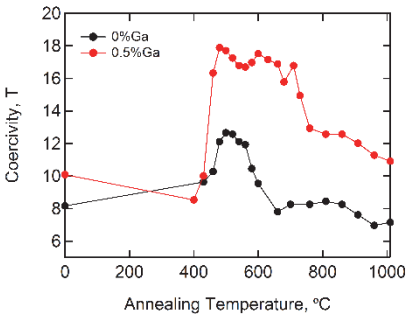


Figure 1: Variations in coercivity ($\mu_0 H_c$) as functions of annealing temperature for Ga-doped and Ga-free samples.

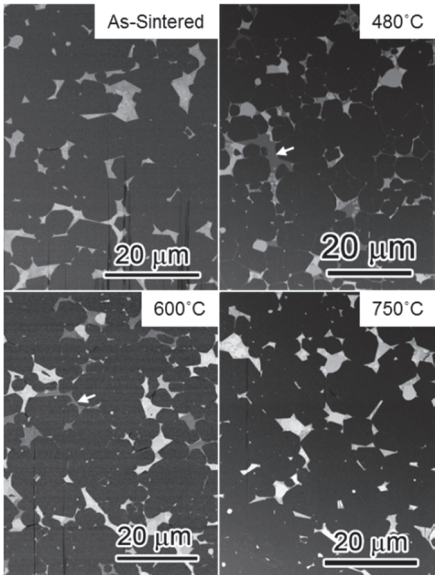


Figure 2: BSE SEM images of as-sintered sample and the samples annealed at 480, 600 750°C. $Nd_6Fe_{13}Ga$ phase is indicated by arrows.

References
1) Hasegawa et al., Abstract for Annual meeting, Japan Society of powder and powder metallurgy, 202 (2013)
2) Yamasaki et al., Abstract for Annual spring meeting, Japan Institute of Metals, S7・21 (2014)

# Scanning soft x-ray magnetic circular dichroism imaging of the changes in magnetic domain structure in Nd-Fe-B sintered magnets throughout the demagnetisation process

D. Billington[1], K. Toyoki[1], Y. Kotani[1], H. Okazaki[1], A. Yasui[1], W. Ueno[1], S. Hirosawa[2], and T. Nakamura[1, 2]

[1]*Japan Synchrotron Radiation Research Institute (JASRI), SPring-8, 1-1-1 Kouto, Sayo 679-5198, Japan.*
[2]*Elements Strategy Initiative Center for Magnetic Materials (ESICMM), National Institute for Materials Science, 1-2 Sengen, Tsukuba 305-0047, Japan.*

One of the most desirable properties of a permanent magnet is a large coercivity, a property that is directly related to the nucleation of reversed magnetic domains and pinning of the domain walls in the bulk of the magnet. In order to understand the relationship between the coercivity and the generation and evolution of magnetic domains, magnetic domain observations throughout the demagnetisation process are essential. In Nd-Fe-B sintered magnets, it has been shown that fractured surfaces largely maintain bulk coercivities, whilst polished surfaces do not [1]. This makes magnetic domain imaging of the fractured surface under applied magnetic fields highly desirable. So far, many magnetic imaging studies of these materials have been reported. However, conventional magnetic microscopes that can operate under magnetic fields are limited to polished surfaces or transmittable thin films, whilst those that can observe the fractured surface cannot operate under magnetic fields. In order to overcome these limitations, we have developed a scanning soft x-ray magnetic circular dichroism (XMCD) microscope with a spatial resolution of about 100 nm and a focal depth of ±5 $\mu$m from the focal point, thereby allowing element specific magnetic domain observations of fractured surfaces. Furthermore, this apparatus is equipped with a superconducting magnet (with a maximum field of ±8 T), which permits investigations of the magnetic field dependence of the magnetic domains. In this talk, I will briefly describe our soft XMCD microscope, and demonstrate its effectiveness by showing some recent results from commercial Nd-Fe-B sintered magnets (see, for example, Fig.1). In particular, I will show and highlight the differences in the magnetisation reversal process in the fractured and polished surfaces of the same sample.

The authors thank T. Nishiuchi and T. Fukagawa from Hitachi Metals, Ltd. for supplying the sample. Part of this work is supported by the ESICMM under the outsourcing project of MEXT.

**References**

[1] T. Nakamura *et al.*, Appl. Phys. Lett. **105**, 202404 (2014).

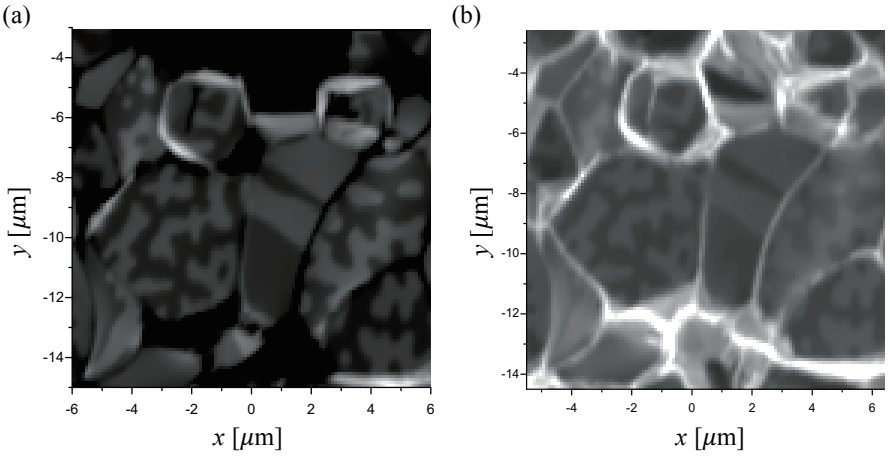


Figure 1: (a) Positive helicity x-ray absorption map of a commercial Nd-Fe-B magnet taken at the Fe $L_3$-edge. (b) Same as (a) but at the Nd $M_4$-edge

# Domain structure of exchange-coupled and exchange-decoupled Nd-Fe-B sintered magnets

M. Soderžnik[1], H. Sepehri-Amin[1], T. Sasaki[1], T. Ohkubo[1], Y. Takada[2], T. Sato[2], Y. Kaneko[2], A. Kato[3], and K. Hono[1]

[1]National Institute for Materials Science, 1-2-1 Tsukuba 305-0047, Japan

[2]Toyota Central R&D Labs., Inc., 41-1, Nagakute 480-1192, Japan

[3]Toyota Motor Corp, Advanced Material Engineering Div., Susono 410-1193, Japan

Understanding the magnetization reversal processes in Nd-Fe-B sintered magnets is important in order to obtain a clue to enhance the coercivity of Nd-Fe-B magnets without using heavy rare earth elements. In order to meet the demand of high coercivity without changing the currently established powder metallurgy route, Nakajima and Yamazaki [K. Nakajima and T. Yamazaki, Japan Patent. (2015) 5767788] reported a new series of sintered magnets that achieve the coercivity of more than 1400 kA/m and the remanence of 1.38 T without refining the grain size. The microstructural characterization revealed well-isolated 2:14:1 grains with Ga-doped Nd-rich intergranular phase[1]. Such non-magnetic intergranular phase with the chemical composition $Nd_6(Fe,Ga)_{14}$ was reported to decouple the ferromagnetic grains and reduce the influence of the reverse domain formation between neighboring grains. In this work, we observed the magnetic domain structure of Ga-doped Nd-rich Nd-Fe-B magnet and the commercial Nd-Fe-B magnet by means of magneto-optical Kerr effect in order to understand the mechanisms of magnetization reversal processes in these two types of magnets. The samples were mechanically polished with the c-axis out of the plane and in the plane. Magnets were first fully saturated in magnetizer with the field of 5 T and then brought to the remanent state. In the commercial magnet, much more grains remained saturated compared to the Ga-doped Nd-rich magnet (a1 and b1). The reason for this is better isolation of 2:14:1 grains in Ga-doped Nd-rich magnet. If the grains are better isolated, each grain feels higher stray field which lead to domain formation on the surface of magnet. When the reverse magnetic field was applied to the magnet, we observed different domain formation. In the commercial magnet cascade-like domain propagation occurred (marked region in a2 and a3). At high-enough field the surface domains of a few grains were switched simultaneously. This implies the grains are exchange-coupled due to the low amount of Nd-rich intergranular phase. On the contrary, in Ga-doped Nd-rich magnet the domain formation was initiated from the boundary and at high-enough field the domains propagated through the whole grain (marked region in b2 and b3).

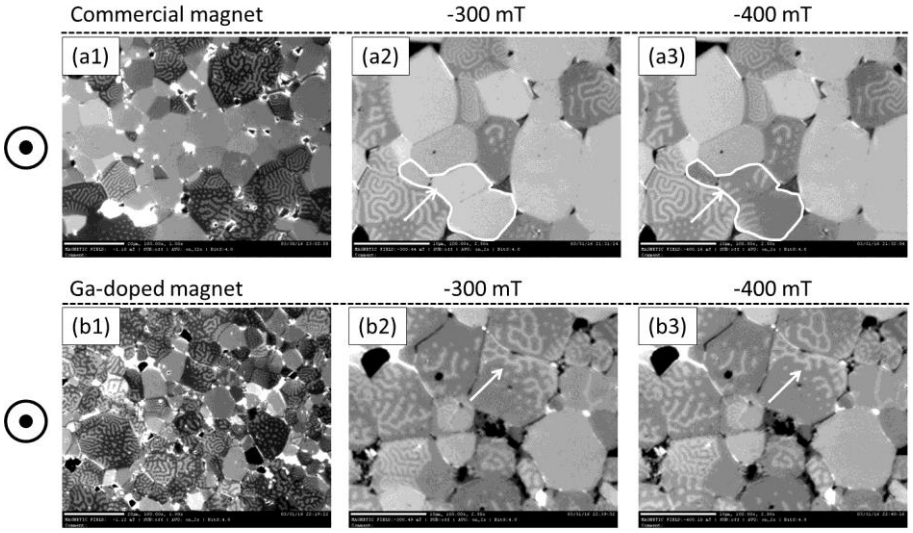


Figure 1: Domain structure in commercial and Ga-doped Nd-rich Nd-Fe-B magnet

[1] T. T. Sasaki, T. Ohkubo, Y. Takada, T. Sato, A. Kato, Y. Kaneko, K. Hono, Formation of non-ferromagnetic grain boundary phase in a Ga-doped Nd-rich Nd-Fe-B sintered magnet, Scripta Materialia 113 (2016) 218–221

# Coercivity enhancement of hot-deformed Nd-Fe-B magnets by the eutectic grain boundary diffusion process

Lihua Liu[a,b], H. Sepehri-Amin[a], M. Yano[c], A. Kato[c], T. Shoji[c], T. Ohkubo[a], and K. Hono[a,b]
[a)]ESICMM, National Institute for Materials Science, Tsukuba 305-0047, Japan
[b)]Graduate School of Pure and Applied Sciences, University of Tsukuba, Tsukuba 305-8577, Japan
[c)]Toyota Motor Corporation, Advanced Material Engineering Div., Susono 410-1193, Japan

The eutectic grain boundary diffusion process was applied to hot-deformed Nd-Fe-B magnets using various types of $Nd_xM_y$ compounds as the diffusion source, where M includes Al, Cu, Ga, Zn, Mn, Co, Ni, and Fe. Formation of non-ferromagnetic Nd-rich intergranular phase was believed as the main reason for remarkable coercivity enhancement, whereas also leads to large degradation in remanent magnetization [1-3]. T.T. Sasaki et al [4] showed that trace amount of Ga doping to Nd-Fe-B sintered magnets could give rise to coercivity of 1.8 T by post annealing with more homogeneous distribution of Nd-rich grain boundary phase. In this work, we used $Nd_{62}Fe_{14}Ga_{20}Cu_4$ at.% alloy as diffusion source, applying to 4 mm thick hot-deformed Nd-Fe-B magnets aiming for an optimal coercivity with high remanent magnetization.

Hot-deformed magnets with the composition of $Nd_{13.2}(Fe,Co)_{bal}B_{4.7}Ga_{0.5}$ (at.%) in 5×5×4 $mm^3$ size were used as the starting materials. The eutectic grain boundary diffusion was carried out by coating the magnets with melted eutectic alloy ribbons, followed by heat treatment at 600°C for 3 hour. The microstructures of the samples were studied using SEM/FIB (Carl ZEISS 1540EsB), TEM (Titan G2 80-200).

Hysteresis loops of the hot-deformed and diffusion-processed magnets are shown in Figure 1. After the heat treatment at 600°C for 1 h by $Nd_{62}Fe_{14}Ga_{20}Cu_4$ diffusion process, coercivity can be increased from 1.26 T to around 2.22 T with a remanence of 1.31 T at room temperature (Fig.1a). The diff. proc. sample can retain the coercivity of around 0.80 T at 160°C. We find the NdFeGaCu diff. proc. sample shows relatively better texture compared with that diff. proc. with Nd-Al compound (Fig.2). Detailed TEM characterization was carried out to figure out the microstructure of grain boundary phase formed after the diffusion process, as well as the interface feature that may contribute to the texture evolution when the diffusion happened.

This work was in part supported by JST, CREST.

**Reference**

[1] H. Sepehri-Amin, T. Ohkubo, T. Nishiuchi, N. Nozawa, S. Hirosawa and K.Hono, Acta Mater, **63**, 1124 (2010)
[2] H. Sepehri-Amin, T. Ohkubo, S. Nagashima, M. Yano, A. Kato, T. Shrefl and K.Hono, Acta Mater, **61**, 6622 (2013)
[3] L. Liu, H. Sepehri-Amin, T. Ohkubo, M. Yano, A. Kato, T. Shoji and K. Hono, J. Alloy. Compd., **666**, 432 (2016)
[4] T. T. Sasaki, T. Ohkubo, Y. Takada, T. Sato, A. Kato, Y. Kaneko and K. Hono, Scr. Mater. 113, **218** (2016)

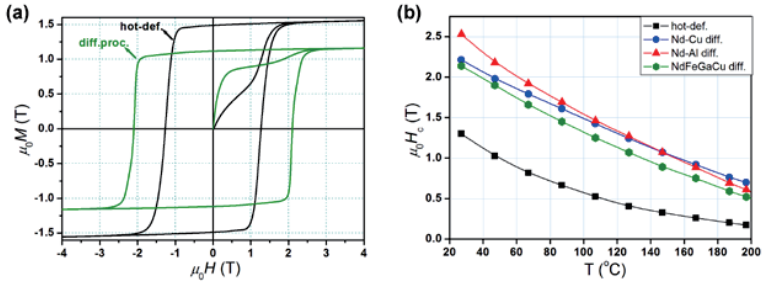


Fig. 1 Hysteresis loops of hot-deformed and NdFeGaCu diff. proc. samples a); temperature dependence of hot-deformed, Nd-Al, Nd-Cu, and NdFeGaCu diff. proc. samples b).

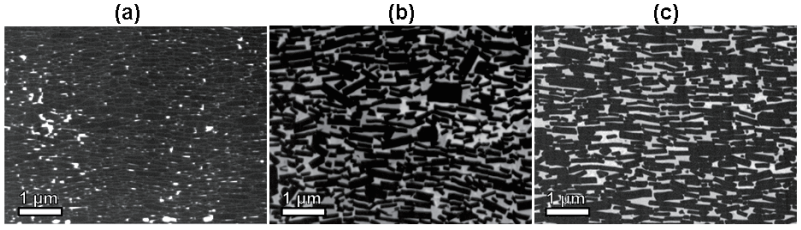


Fig. 2 BSE-SEM images of hot-deformed a), Nd-Al diff. proc. b) and NdFeGaCu diff. proc. samples c).

# Coercivity enhancement in hot deformed Nd-Fe-B magnets processed from amorphous precursors

Xin Tang,[1,2] H. Sepehri-Amin,[1] T. Ohkubo,[1] K. Hioki,[3] A. Hattori[3] and K. Hono[1,2]
[1]Elements Strategy Initiative Center for Magnetic Materials, National Institute for Materials Science, Tsukuba 305-0047, Japan
[2]Graduate School of Pure and Applied Sciences, University of Tsukuba, Tsukuba 305-8577, Japan
[3]Daido Corporate Research & Development Center, Daido Steel Co., Ltd.

The hot-deformed magnets have attracted considerable interests since Lee reported their highly-anisotropic and ultrafine-grained microstructure features in 1985.[1)] Given the small grain size (~400 nm) in hot-deformed magnets, the coercivity is expected to be as high as ~2.5 T. However, experimental values are much lower.[2)] The coercivity is extremely sensitive to microstructure, such as the chemical composition of intergranular phase and the aspect ratio (ratio between length along ab plane and length along c plane: $L_{ab}/L_c$) of grains. These microstructural features change depending on processing conditions. In this paper, we processed hot-deformed magnets from amorphous and nanocrystalline precursors and compared their microstructures and coercivities to explore the optimum processing route to maximize the coercivity.

The crystal and amorphous powders with composition of $Nd_{28.3}Pr_{0.06}Fe_{bal}Co_{3.41}Ga_{0.53}Al_{0.06}B_{0.97}$ (wt.%) were produced by melt-spinning with different cooling rates. These two kinds of powders were compacted by hot pressing at 650°C in vacuum, which were subsequently hot-deformed at 850 °C until 75% height reduction were achieved. The magnetic properties and microstructure were studied by BH tracer and SEM/FIB (Carl ZEISS 1540EsB), respectively.

Fig. 1 shows the demagnetization curves of hot deformed magnets processed from nanocrystalline and amorphous powders. By processing magnets from amorphous powders, the coercivity can be increased from ~1.28 T to ~1.4 T, while keeping the remanence at 1.42 T, which is resulted from optimized microstructure in this sample as indicated in Fig. 2. In Fig.2, the aspect ratio of $Nd_2Fe_{14}B$ grains in hot-deformed magnets processed from amorphous precursors is calculated to be ~0.43, which is reduced to ~0.32 in the counterpart processed from amorphous precursors. Consequently, grains in the sample produced from nanocrystalline precursors present more feature of elongated shape, suggesting bigger effective demagnetized factor and lower coercivity. STEM/EDS studies of the intergranular phase suggested the Nd-concentration in the sample fabricated from the amorphous precursor is higher than that processed from nanocrystalline precursor.

## Reference

1) R.W. Lee, Appl. Phys. Lett. **46** (1985) 790.
2) K.Hono, H. Sepehri-Amin, Scri. Mater. **67** (2012) 530.

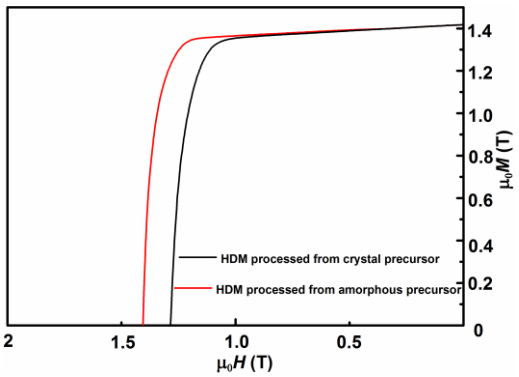


Fig. 1 Demagnetization curves of hot deformed magnet (HDM) processed from nanocrystalline and amorphous precursors.

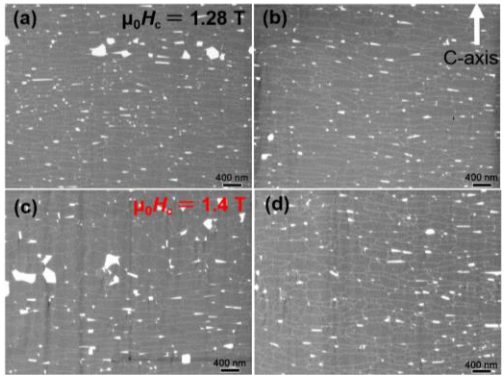


Fig. 2 BSE-SEM images of the hot-deformed magnets processed from nanocrystalline precursor (a,b) and amorphous precursor (c,d).